Structural Stiffness Characteristics of the Solid Rocket Booster Field Joint

Dan A. Bodeker, III
Graduate Research Assistant
Aerospace Engineering

Dr. Winfred A. Foster, Jr.
Professor
Aerospace Engineering

Auburn University
211 Aerospace Engineering Building
Auburn, AL 36849-5112

Prepared For:
National Aeronautics and Space Administration
George C. Marshall Space Flight Center
Marshall Space Flight Center, AL 35812

Contract
NAS8-39131-DO29

November 13, 1998

Abstract

The Space Shuttle Solid Rocket Booster (SRB) is a complex assembly of segments of which the field and factory joints contain an unpredictable amount of freeplay. Freeplay is inherent due to tolerances in being able to assemble the segments and the gaps that occur at each joint. The purpose of this work is to quantify the amount of freeplay for the field joint as well as identify the effects of introducing multiple joints that contain freeplay into a system. To provide a baseline for the above study an additional model was made to quantify the behavior of a field joint that does not have any freeplay in the system.

Structural Stiffness Characteristics of the Solid Rocket Booster Field Joint

Dan A. Bodeker, III
Graduate Research Assistant
Aerospace Engineering

Dr. Winfred A. Foster, Jr.
Professor
Aerospace Engineering

Auburn University
211 Aerospace Engineering Building
Auburn, AL 36849-5112

Prepared For:
National Aeronautics and Space Administration
George C. Marshall Space Flight Center
Marshall Space Flight Center, AL 35812

Contract
NAS8-39131-DO29

November 13, 1998

Table of Contents

ABSTRACT ii

LIST OF FIGURES iv

LIST OF TABLES vi

1. INTRODUCTION 1

2. BACKGROUND 1

3. MODEL DESCRIPTION 4

3.1 TANG MODEL 5

3.2 CLEVIS MODEL 6

3.3 PIN MODEL 5

3.4 INTERFACES 6

4. LOAD CASES 8

4.1 MATERIAL PROPERTIES 8

4.2 CONSTRAINTS 8

4.3 NASTRAN NON-LINEAR SOLUTION 8

4.4 NON-LINEAR FREEPLAY LOAD CASES 9

4.5 NON-LINEAR MODIFIED GAP LOAD CASES 9

5.0 RESULTS 9

5.1 DISPLACEMENTS 9

5.2 VON MISES STRESS 11

6.0 CONCLUSIONS 11

7.0 REFERENCES 13

APPENDIX A A-1

APPENDIX B B-1

LIST OF FIGURES

FIGURE 1. RSRM SEGMENT CONFIGURATION 1
FIGURE 2. SRB TWANG TEST CONFIGURATION 2
FIGURE 3. EXAMPLE OF FREEPLAY 4
FIGURE 4. SRB REDESIGNED FIELD JOINT 5
FIGURE 5. PIN GAP ELEMENTS 5
FIGURE 6. SRB FINITE ELEMENT PIN MODEL 6
FIGURE 7. SRB FINITE ELEMENT TANG WITH CAPTURE FEATURE 7
FIGURE 8. SRB FINITE ELEMENT CLEVIS MODEL 7
FIGURE 9. PERCENTAGE CONTRIBUTION OF FREEPLAY 10
FIGURE A-1. A) RADIAL DEFLECTION. (IN.) B) AXIAL DEFLECTION. (IN.)...A-2
FIGURE A-2. VON MISES STRESS CONTOURS FOR JOINT. (PSI) A-3
FIGURE A-3. VON MISES STRESS CONTOURS FOR CLEVIS. (PSI) A-4
FIGURE A-4. VON MISES STRESS CONTOURS FOR PIN. (PSI) A-5
FIGURE A-5. VON MISES STRESS CONTOURS FOR TANG. (PSI) A-6
FIGURE A-6. A) RADIAL DEFLECTION. (IN.) B) AXIAL DEFLECTION. (IN.) ...A-7
FIGURE A-7. VON MISES STRESS CONTOURS FOR JOINT. (PSI) A-8
FIGURE A-8. VON MISES STRESS CONTOURS FOR CLEVIS. (PSI) A-9
FIGURE A-9. VON MISES STRESS CONTOURS FOR PIN. (PSI) A-10
FIGURE A-10. VON MISES STRESS CONTOURS FOR TANG. (PSI) A-11
FIGURE A-11. A) RADIAL DEFLECTION. (IN.) B) AXIAL DEFLECTION. (IN.)A-12
FIGURE A-12. VON MISES STRESS CONTOURS FOR JOINT. (PSI) A-13
FIGURE A-13. VON MISES STRESS CONTOURS FOR CLEVIS. (PSI) A-14
FIGURE A-14. VON MISES STRESS CONTOURS FOR PIN. (PSI) A-15
FIGURE A-15. VON MISES STRESS CONTOURS FOR TANG. (PSI) A-16
FIGURE B-1. A) RADIAL DEFLECTION. (IN.) B) AXIAL DEFLECTION. (IN.)...B-2
FIGURE B-2. VON MISES STRESS CONTOURS FOR JOINT. (PSI) B-3
FIGURE B-3. VON MISES STRESS CONTOURS FOR CLEVIS. (PSI) B-4
FIGURE B-4. VON MISES STRESS CONTOURS FOR PIN. (PSI) B-5

FIGURE B-5. VON MISES STRESS CONTOURS FOR TANG. (PSI) B-6
FIGURE B-6. A) RADIAL DEFLECTION. (IN.) B) AXIAL DEFLECTION. (IN.) ... B-7
FIGURE B-7. VON MISES STRESS CONTOURS FOR JOINT. (PSI) B-8
FIGURE B-8. VON MISES STRESS CONTOURS FOR CLEVIS. (PSI) B-9
FIGURE B-9. VON MISES STRESS CONTOURS FOR PIN. (PSI) B-10
FIGURE B-10. VBN MISES STRESS CONTOURS FOR TANG. (PSI) B-11
FIGURE B-11. A) RADIAL DEFLECTION. (IN.) B) AXIAL DEFLECTION. (IN.)B-12
FIGURE B-12. VON MISES STRESS CONTOURS FOR JOINT. (PSI) B-13
FIGURE B-13. VON MISES STRESS CONTOURS FOR CLEVIS. (PSI) B-14
FIGURE B-14. VON MISES STRESS CONTOURS FOR PIN. (PSI) B-15
FIGURE B-15. VON MISES STRESS CONTOURS FOR TANG. (PSI) B-16

LIST OF TABLES

TABLE 1 - TWANG TEST Z-DIRECTION DISPLACEMENTS 3
TABLE 2 - RADIAL DEFLECTION OF NODE 20 9
TABLE 3 - SRB MASS PROPERTIES AND FREEPLAY 10
TABLE 4 - VON MISES STRESS DISTRIBUTION 11

1. INTRODUCTION

The Space Shuttle Solid Rocket Booster (SRB) is assembled at the Kennedy Space Center (KSC) in Cape Canaveral, Florida. Each of the two SRBs used during a launch consists of four solid rocket motor sections mated together using equally spaced pins. The segments are assembled using a series of field joints and factory joints (Figure-1). The field joint differs by incorporating a capture feature with an additional O-ring in the tang. This was developed for safety purposes as a result of the Challenger accident.

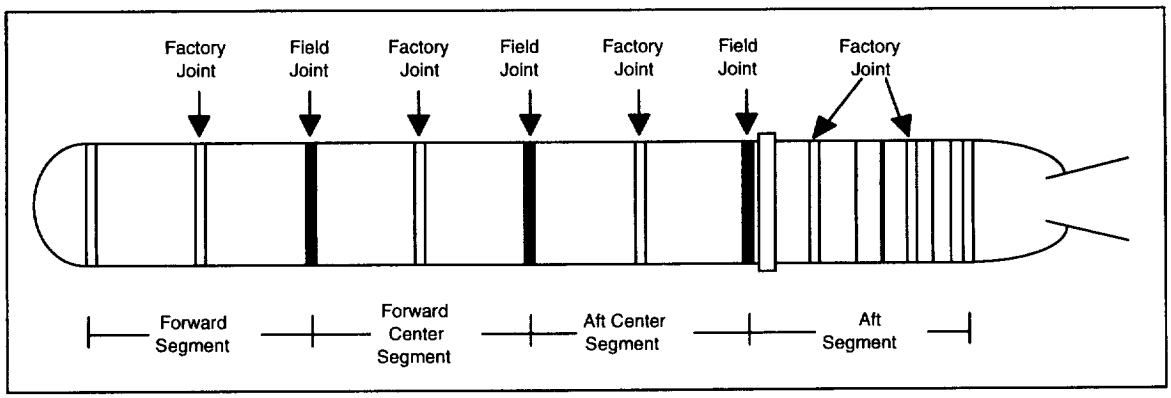

Figure 1 - RSRM Segment Configuration

This report contains the results of a detailed finite element analysis of the Solid Rocket Booster (SRB) field joint between the forward segment and the forward center segment. Previous analysis has mainly focused on the effects of launch and flight loads on the gap openings for the internal O-rings inside the joint. The analysis contained herein focuses on determining the structural stiffness as well as the effect of freeplay on the joint for use in analytical models of the Space Shuttle system.

The finite element model provides an analysis of the joint based on nominal tolerances as detailed in SRB drawings. To gain further understanding of freeplay, additional models of the joint are made that remove the freeplay from the system. These models serve as a baseline for the joint analysis under a given compressive load.

2. BACKGROUND

The stiffness of the SRBs can be observed during the Space Shuttle Main Engine (SSME) ignition sequence. At T-6.6 seconds, the SSMEs are ignited prior to SRB ignition. Due to the SRBs being constrained to the launch pad, an overturning moment causes the SRBs to lean in a direction opposite of the thrust at an angle of approximately 1 degree. The elastic nature of the SRBs then causes the boosters to rock back towards the vertical position. Once the boosters reach the vertical position the boosters are ignited. This phenomena is basically referred to as the pre-liftoff "twang" effect.

To measure this phenomenon, strain gauges at the hold-down posts measure the amount of force exerted on the aft skirt at SSME build-up. This coupled with video of the tip

deflection of the External Tank (ET) during "twang" provides an idea of how stiff the SRBs are. Each launch can produce slightly different results due to varying details, i.e, payload, SSME build-up, atmospheric conditions, etc.

Due to varying conditions on the launch pad, the best possible opportunity to determine the stiffness characteristics of the SRBs is during assembly in the Vehicle Assembly Building (VAB). The SRBs are stacked a segment at a time on a Mobile Launch Platform (MLP) with an aft skirt as the interface. The segments are joined together using 177 load bearing pins and three additional alignment pins to ensure proper mating. Prior to mating the two SRBs with the External Tank (ET) at the forward attach interface, the SRBs are pulled apart a specified distance to ensure proper clearance. Strain gauges on the hold-down posts as well as dial gauges where the SRBs are pulled apart provides an indication of how much force is required to cause a specific deflection.

In March of 1979, an SRB twang test was performed on a full scale SRB (1388.567 inches) to verify top-level program requirements documenting the SRB stiffness (Figure 2). The primary goal of the test was to measure the first Z bending mode of the SRB on the MLP. The secondary goal was to verify the Z-direction bending stiffness. Five different load cases were used and measurements were taken both optically and with a steel gauge.

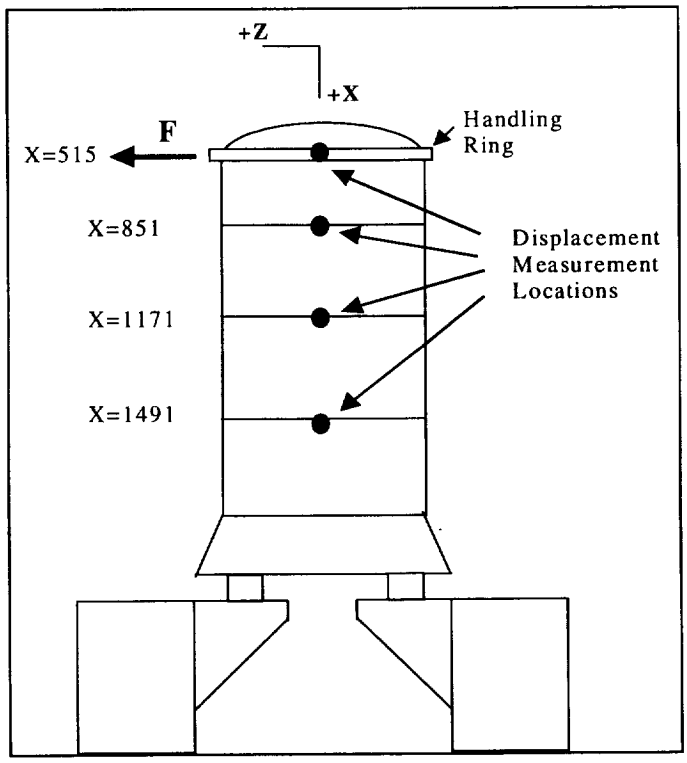

Figure 2 - SRB Twang Test Configuration

The results showed that a 10,000 pound load applied to the SRB would result in a .65 in. displacement. This translated into a stiffness of the SRBs in the Z direction of 15384.6 lbs/in. However, there is still much discrepancy pertaining to the actual number

measured. There were many meetings to discuss the actual number (if the measure number was .65 in or .64 in.) and in fact 15034 lbs/in. is typically used as the correct number. Measurements were taken at each joint along the booster for each applied load in the Z direction (Table 1).

Load (Pounds)	Steel Scale	Optical			
		Fwd	Fwd Center	Aft Center	Aft
1000	0.10	0.05	0.05	-0.05	-0.05
2500	0.16	0.15	0.10	0.07	0.00
5000	0.32	0.32	0.25	0.15	-0.03
7500	0.48	0.48	0.30	0.20	-0.01
10000	0.65	0.65	0.40	0.35	0.00

Table 1 - Twang Test Z-Direction Displacements

The SRBs are less stiff in the Y-direction. This is due in part to the geometry of the hold-down posts as well the design of the stiffener rings on the aft section of the SRBs. The Y-direction stiffness is documented as a requirement to be less than .76 in of displacement with a 10,000 lb. load applied. Mathematical models developed by USBI predicted a displacement of approximately .80 in. for a 10,000 lb. load. In 1993, using finite element modeling methodology obtained from the Advanced Solid Rocket Motor (ASRM) program, the current SRBs had a predicted displacement of .88 in. or 10% less stiff.

In 1992, a database was created to identify the amount of force required to separate the SRBs (Y-direction) and the amount of distance the SRBs moved during mating. After studying several SRB pull operations, it was determined the stiffness varied significantly from 4500 lb/in. to over 12,000 lb/in. This number was based on measurements performed by KSC assembly personnel using a dynamometer (load) and a dial indicator (displacement) attached to a temporary floor.

As a result of several SRB pull operations, data that was collected identified some of the major contributions to the large stiffness discrepancy. The configuration of the system used to separate the boosters was identified as producing significant error. The location of the dial indicator assembly on a retractable platform may have contributed to some error as well. Some of the mating procedures were identified as being incorrect for some of the cases where data was collected. Once these problems were identified and corrected, future measurements resulted in more accurate predictions of SRB stiffness.

Additional factors still remain in determining stiffness as well the contribution of freeplay. The SRBs are assembled using three field joints and seven factory joints. At the

interface between the aft motor segment and aft skirt is an additional pin joint. The aft skirt serves as the interface between the Shuttle system and the MLP.

Studying the tang and clevis joint in further detail reveals two effects: freeplay and stiffness. The large diameter of the SRBs requires a certain tolerance to ensure the segments can be mated during assembly. The tolerances add up to gaps between segments as they are mated. This is referred to as the freeplay of the joint. An example of this would be a bar inside a cup (Figure 3). An initial position of the bar, 1, that has a negligible force applied will cause a + or - displacement, d, as shown below to the new position. This displacement will occur without influence from the material properties of the bar except for mass.

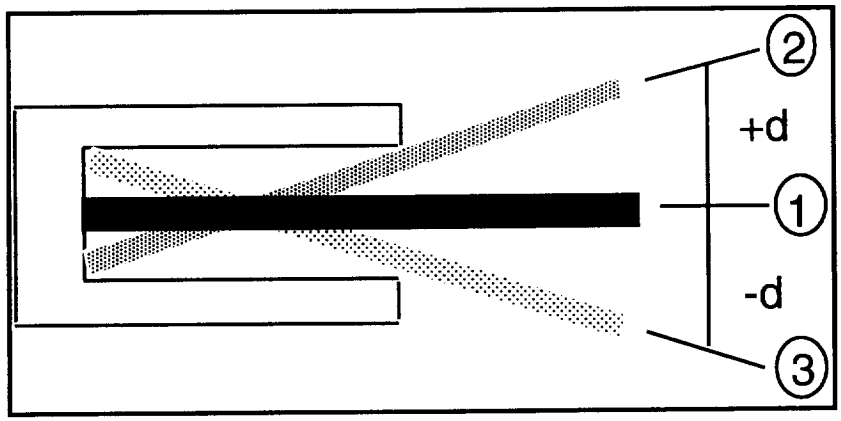

Figure 3- Example of Freeplay

Once the bar has reached position 2 or 3, the amount of force required to produce a displacement becomes the typical force-displacement slope where the slope is a function of the material properties of the bar. For the field joint, once the freeplay is removed from the joint through contact, the stiffness of the design is a result of the material properties and load paths.

The following sections provide details on the design of the SRB tang and clevis field joint. A detailed one-degree segment model is constructed and subjected to compressive and shearing loads. The stiffness of the joint is also compared to the same joint design that has no freeplay. This was done by changing the stiffness of the gap elements to a much larger stiffness than that of the joint in an open and closed condition.

3. MODEL DESCRIPTION

The field joint used for this analysis was a standard weight cylinder (forward segment) mated to a lightweight cylinder (forward center segment) located at SRB station 851.5. The mating surface of the standard weight cylinder is referred to as the tang with capture feature. The lightweight cylinder-mating surface is called the clevis (Figure 4).

The model was built using PATRAN as a pre- and post-processor to generate the NASTRAN finite element code. The model was drawn to scale in two dimensions using

nominal tolerances from the RSRM approved drawings. The radius from the centerline of the booster provided the pivot point for creating the three dimensional model.

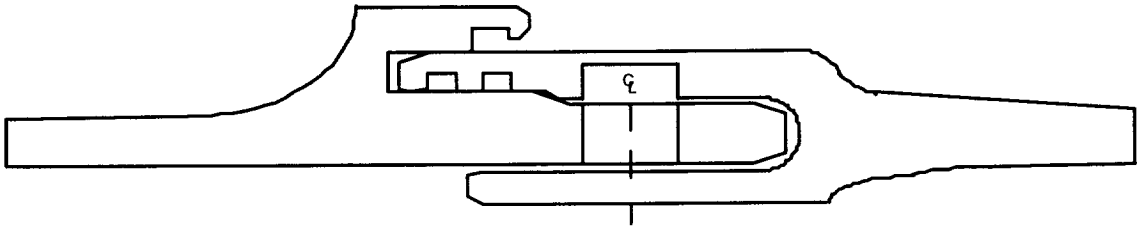

Figure 4 - SRB Redesigned Field Joint

After the geometry of the 2D model was completed, QUAD4 elements were used to develop the initial mesh for the model. Some triangular elements, TRIA3, were used on the clevis and the pin model. Once the 2D mesh was completed, the 2D model was swept 1 degree clockwise based on the approximate case segment radius of 72.3135 inches to create a 3D model using HEX8 elements. The initial 3D mesh did not include the pin model. The geometry of the pin was created and a corresponding mesh was developed that would align with the tang and clevis mesh. Gap elements were used between the pin and the tang and clevis and adjusted so that contact surfaces existed as represented by the arrows in the figure below. The minimum clearance is 0.00 in. while the maximum gap tolerance is 0.0054 in. (Figure 5).

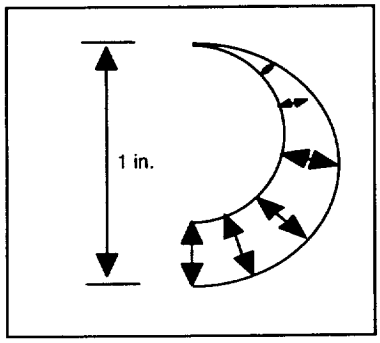

Figure 5 - Pin Gap Elements

3.1 Pin Model

The 3D pin model was created using approximately 1300 HEX8 elements and an additional 2000 nodes (Figure 6). Wedge elements were used to model the area of the pin hole used to retract pins from the SRB during demating procedures.

3.2 Tang Model

The tang with capture feature was created using nominal dimensions from RSRM drawings. The standard weight cylinder dimensions were obtained from RSRM drawing 1U52983. The tang mating surface is a part of the forward case segment of the SRB. The 3D model was created with over 2200 HEX8 elements and approximately 3400 nodes (Figure 7). Gap elements were used about the circumference of the pin hole cutout as identified in Figure 5.

3.3 Clevis Model

The clevis was modeled using nominal dimensions from RSRM drawing 1U50717. It represents the mating surface of the forward center segment of the SRB. Approximately 2300 HEX8 elements were used to model the clevis as well as over 4300 nodes (Figure 8). An additional 23 wedge elements were included to interface with the back surface of the pin.

3.4 Interfaces

Gap elements were used extensively throughout the model where there was a predicted load path. There are many locations where two surfaces have contact and to prevent them from being equivalenced and forming one surface gap elements were used. The modulus of the gap elements when closed is 2.9E10 lb/in. Additionally, multipoint constraints (MPCs) were used to represent the shim placed between the clevis and tang to reduce the amount of freeplay.

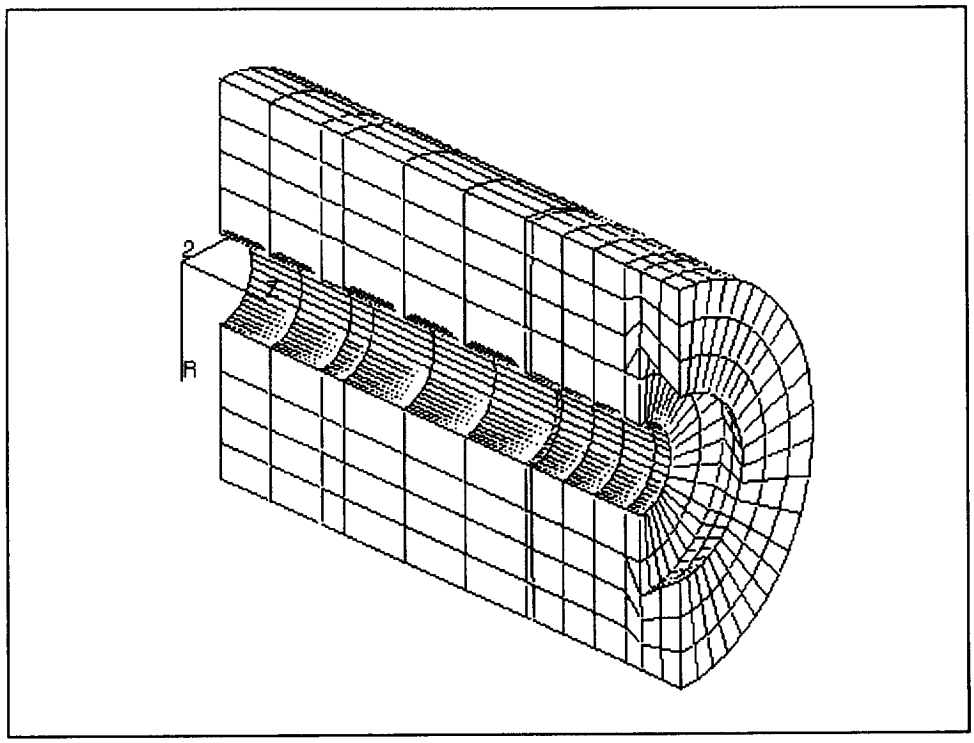

Figure 6 - SRB Finite Element Pin Model

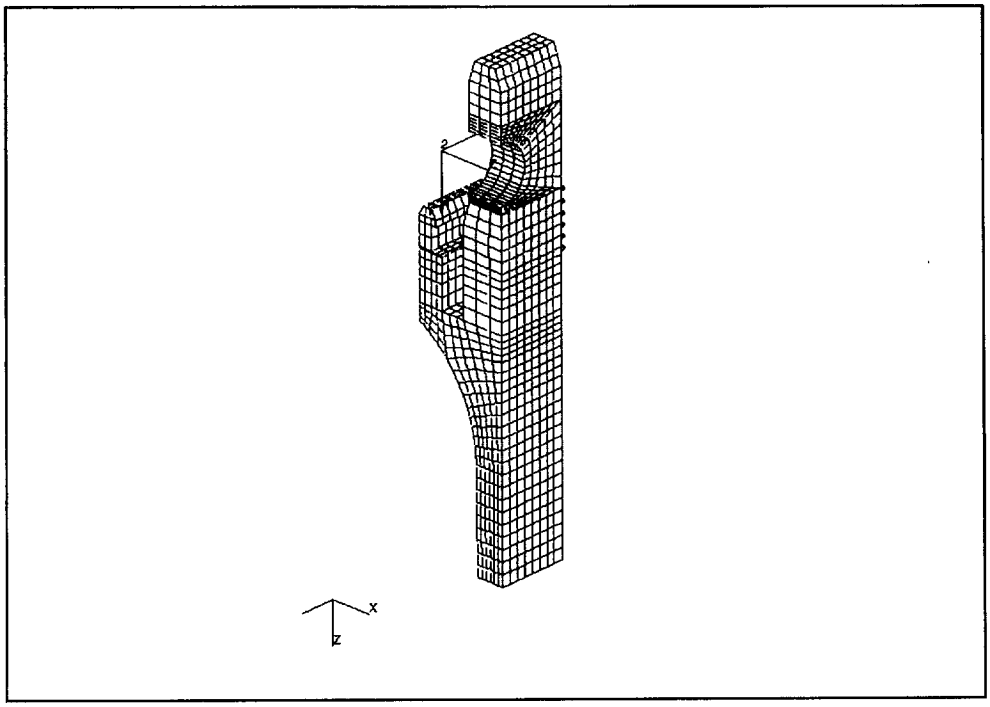

Figure 7 - SRB Finite Element Tang with Capture Feature

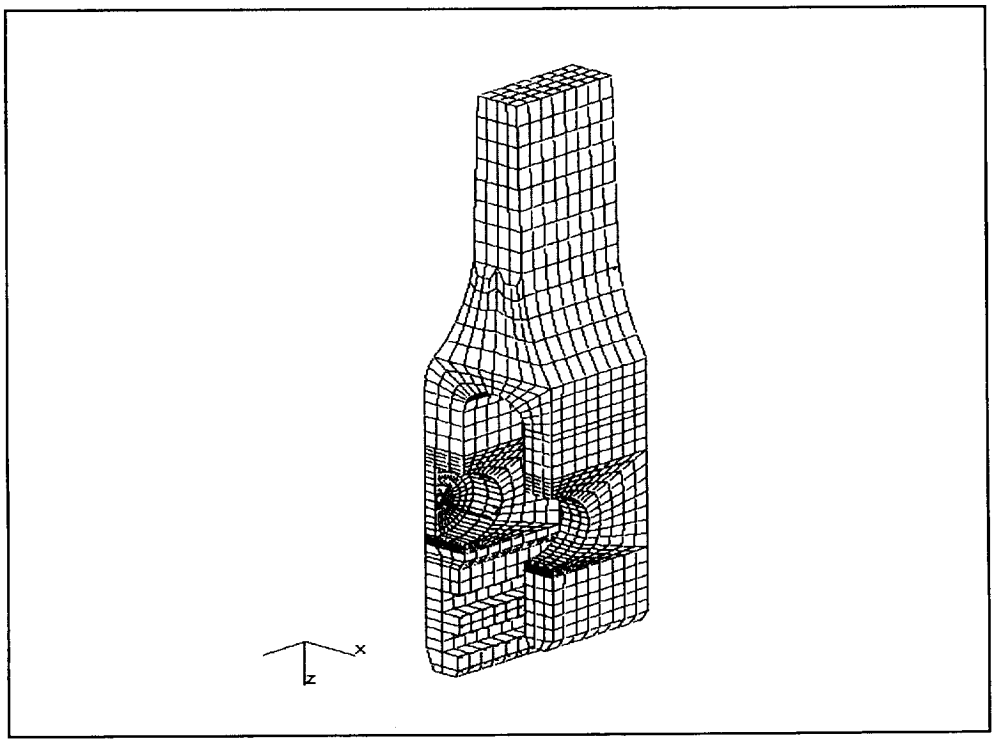

Figure 8 - SRB Finite Element Clevis

4. LOAD CASES

Two types of analysis were used to characterize the amount of freeplay in the model. The first analysis focused on using a non-linear solution with freeplay. Additional non-linear solutions were also run to identify the stiffness of the joint if freeplay was absent from the system. To replicate the load case used during the SRB twang test, a coupled load is applied to the joint in both the axial and radial directions. Additionally, there is a 50 psi load applied to the pin to represent the force of the pin retainer band.

4.1 Material Properties

The tang and clevis are both made from high strength D6AC steel alloy. D6AC has a Young's modulus of 29.6E6 and a Poisson's ratio of .32. The load bearing pins are made out of a nonferrous MP35N nickel alloy with a Young's modulus of 31.5E6 and a Poisson's ratio of .29.

For the analysis with freeplay, the gap elements have a modulus of 29.6E10 when closed and 2.9E-4 when open. For the analysis without freeplay, the gap elements have a stiffness of 2.9E10 for both the open and closed states.

4.2 Constraints

There are three different constraints applied to the model. All elements were constrained from rotation since solid elements only have stiffness in the translation degrees of freedom. The model was constrained in all degrees of freedom at the bottom surface of the joint. The circumferential 0° and 1° planes were constrained from translation in the circumferential direction to enforce symmetric deformations.

4.3 NASTRAN Non-Linear Solution

The non-linear static solution type used for this analysis was Solution 106. The primary uses for this solution type are to support analysis of models with geometric and material non-linearity as well as contact problems. The solutions obtained for this type of analysis are based on an iterative procedure and use convergence criteria based on displacement, work, energy or a combination of these criteria. Important in the non-linear solution is the number, i.e., size of the load steps (increments) which are used. The number of load steps may vary depending on the load size and the results of previous runs. Convergence of some load steps can be difficult to achieve and may require modification to the load step increment or convergence criteria.

The non-linear analysis allows the use of adaptive gap elements to model point-to-point contact. When gap elements are open, there is no contact or friction. When the gap element is closed, sliding (no friction), sticking (static friction), or slipping (kinetic friction) can be modeled. For this analysis contact was represented by static friction with a large axial gap stiffness when closed.

4.4 Non-Linear Freeplay Load Cases

The first set of load cases utilized the capability of the gap elements to represent the space between the tang, clevis, and pin where there was no contact or where the surfaces would potentially be separated. A 50 psi pressure load was applied to the pin surface. Three different compression loads were applied to the top of the joint: 1000 psi, 2500 psi, and 5500 psi. Additionally, a 500 lb shear force was applied in +R direction.

4.5 Non-Linear Modified Gap Load Cases

These load cases were the same as listed above with the exception of the gap elements. The gap elements were modified to have a large stiffness (2.9 E10) if either the open or closed condition existed. This would simulate the stiffness of the joint if freeplay was absent from the system.

5.0 RESULTS

The following sections summarize the results for the analysis with freeplay and those without freeplay. Appendix A contains graphical data of the freeplay load case for both displacement and Von Mises stress. Appendix B contains the fringe plots for the case without freeplay for both displacement and Von Mises stress. Both appendices show results for the individual components of the joint.

5.1 Displacements

The freeplay was determined for the joint by considering the radial deflection of the top surface due to an applied bending load. The following table provides a comparison of the radial deflection of the two load cases for Node 20, located on the top of the model, as a function of the applied compressive load and a constant shear load.

Load_Case	1000 lb.	2500 lb.	5500 lb.
Load_Case_A (Freeplay)	0.0426482900	0.0381330600	0.0333777300
Load_Case_B (No Freeplay)	0.0280869600	0.0288460700	0.0303607100

Table 2 - Radial Deflection of Node 20

To determine the contribution of freeplay to the joint, a ratio of the above displacements is calculated. This provides a percentage of the displacement due to freeplay. The percentage is however a function of the shear load applied. Dividing this percentage by the applied shear load provides a percentage of the contribution of freeplay as a function of compression load per pound of shear load applied (Figure 9).

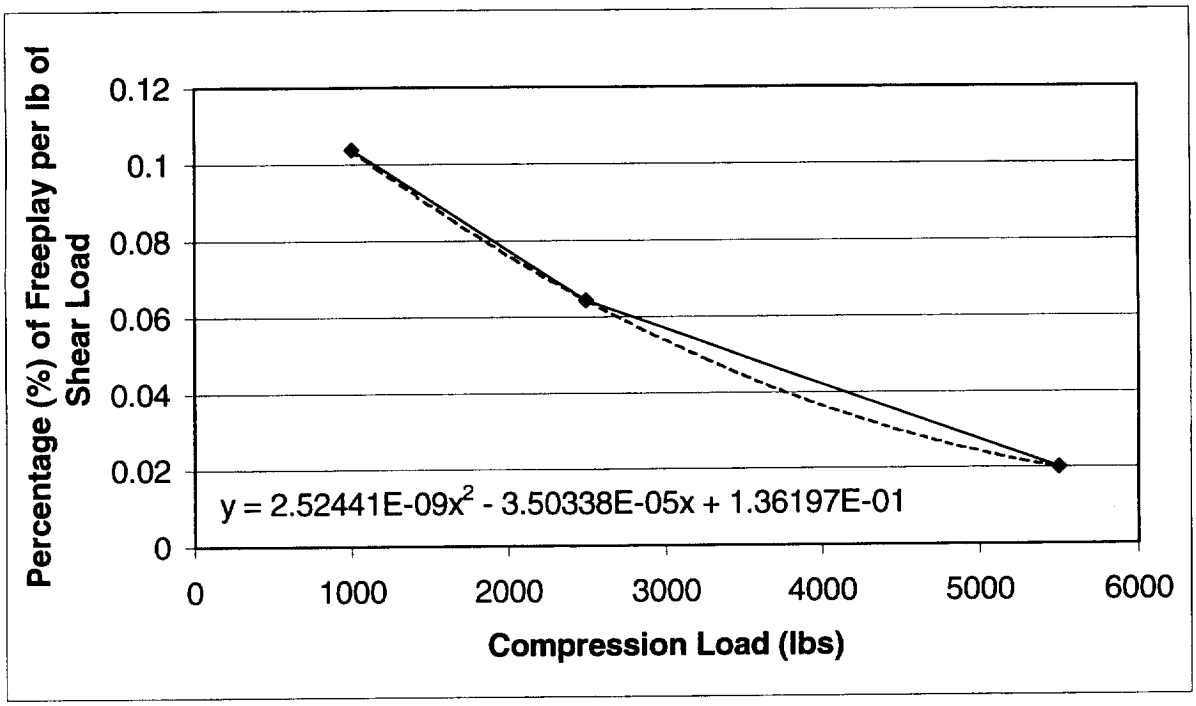

Figure 9 - Percentage Contribution of Freeplay

From the figure above, the contribution of freeplay at each joint can be determined. Assume during the SRB twang test the 10000 lb shear load was distributed circumferentially about the SRB, the result would be a 27.778 lb applied shear load per degree. The shear load is assumed constant along the length of the SRB at each joint.

The following table provides approximate compressive loads for each joint for a full 360 degree condition and a corresponding 1 degree model condition. Based on the approximate SRB mass properties (propellant and case mass) and using Figure 9 it is possible to determine the percentage of freeplay at each joint (Table 3).

Joint Location	Mass (lb)	360° Load (lb)	1° Load (lb)	% Freeplay
Fwd - Fwd Center Joint	333000	333000	925	2.943
Fwd - Aft Center Joint	297000	630000	1750	2.295
Aft Center - Aft Joint	297000	927000	2575	1.742

Table 3 - SRB Segment Mass Properties and Freeplay

The data in Figure 9 was extrapolated using a quadratic fit representation. The one degree load was determined by dividing the sum of the segment mass above the joint by 360. The equation for solving the percent of freeplay contribution for any compression load case can be done by solving the following:

$$\% \text{ of Freeplay} = 2.52441E\text{-}09x2 - 3.50338E\text{-}05x + 1.36197E\text{-}01,$$

where x is the compression load on the joint.

5.2 Von Mises Stress

Additional output from the model included fringe plots of the Von Mises stress for both load cases. Stress fringe plots provided insight to the load path for both analysis. For the case with freeplay, the most significant stress concentrations occurred around the pin location as expected. For the non-freeplay case, significant stress concentrations were observed where the capture feature separates from the tang. Refer to the Appendices for the Von Mises fringe plots. Table 4 below lists the maximum and minimum Von Mises stress for each load case.

Load Case	Maximum	Minimum
Load_A_1000 lb	2.50E+04	1.06E+01
Load_A_2500 lb	2.10E+04	3.65E+01
Load_A_5500 lb	2.53E+04	1.00E+02
Load_B_1000 lb	8.13E+05	1.50E+03
Load_B_2500 lb	8.13E+05	1.59E+03
Load_B_5500 lb	8.13E+05	1.40E+03

Table 4 - Von Mises Stress Distribution

6.0 CONCLUSIONS

The primary focus of this analysis was to characterize and quantify the effect of freeplay on the SRB field joint. This analysis has shown that there is significant coupling within the structure. As the compressive load on the joint increases the net effect on freeplay due to a shear load decreases. Observing the percentage of freeplay contribution on the SRB with an additional 500,000 lbs would reduce the contribution of freeplay at the lowest joint to 1.013% of the displacement.

The coupling of the field joint with freeplay has a significant effect on the joint. With the shear load applied to the joint without freeplay, the radial displacement is almost linear. As the joint with freeplay is subjected to increasing compressive loads, the radial displacement decreases significantly.

Comparing these percentages with the SRB twang test conducted, it is predicted that the freeplay contributed 2.78% of .48 in of displacement at the fwd joint, 2.37% of the .35 in of displacement at the center joint. There was no displacement measured at the aft field joint, which supports the fact that as joint compressive load increases the radial displacement decreases. It is important to note that the deflection measured during the SRB twang test were done in the Z-direction of the booster. There is a significant difference is the stiffness of the SRBs in the Z- and Y- direction.

Additionally, the SRBs in the pre-launch configuration with the added weight of the Space Shuttle and External Tank with fuel significantly increases the compressive force on the SRBs. During SSME build-up, the engines do not exert enough force during twang to unload the joints. The ignition of the SRBs and the subsequent two minutes of ascent flight maintain a large compressive force on the joints.

To fully characterize the effect of freeplay on the system would require additional analysis of the joint with internal pressure line loads, launch loads, and a more accurate representation of the SRM mass properties. The need for knowledge concerning the freeplay and its contribution to displacement is most important during SSME build up and during launch to see the effect on the o-rings. In particular, its potential effect on o-ring seals is of interest.

Additional research should be completed to identify the behavior of the coupling within the field joint. A model of the SRB factory joint, which comprises five other joints on the SRB, should be completed to identify its contribution to the freeplay of the SRB. These two models together can identify the percentage of freeplay for each joint and can be summed over the length of the booster. Additional data should be collected during SRB pull operations to identify at the field joints the radial displacement and used in conjunction with this field joint model and a factory joint model.

7.0 References

Bodeker, D. A., "Solid Rocket Booster Pull Operations", Rockwell Int., June 30, 1993

Brolliar, R. S., "Advanced Solid Rocket Booster Dynamic Math Models", USBI, August 2, 1993

Brolliar, R. S., "Solid Rocket Booster Dynamic Math Models", USBI, August 19, 1994

Bugg, F., "Evaluation of RSRB Cycle II Loads and Dynamic Models", MSFC, April 21, 1993

Bugg, F., "Evaluation of Pre-STS-1 Twang Test Data & Validity of ASRB Model", MSFC, June 7, 1993

Harnett, G. E., "Review of Pre-STS-1 Twang Test Results", Rockwell Int., June 7, 1993

Lohrli, L. E., "Space Shuttle Separation Systems Data Book Section 2: Liftoff", Rockwell Int., August 4, 1992

Stratton, T. C. and Call, V. B., *RSRM Case Structural Analysis Field Joint* Brigham City, Utah: Thiokol Corporation (TWR-17118 Supplement B), 1995

APPENDIX A

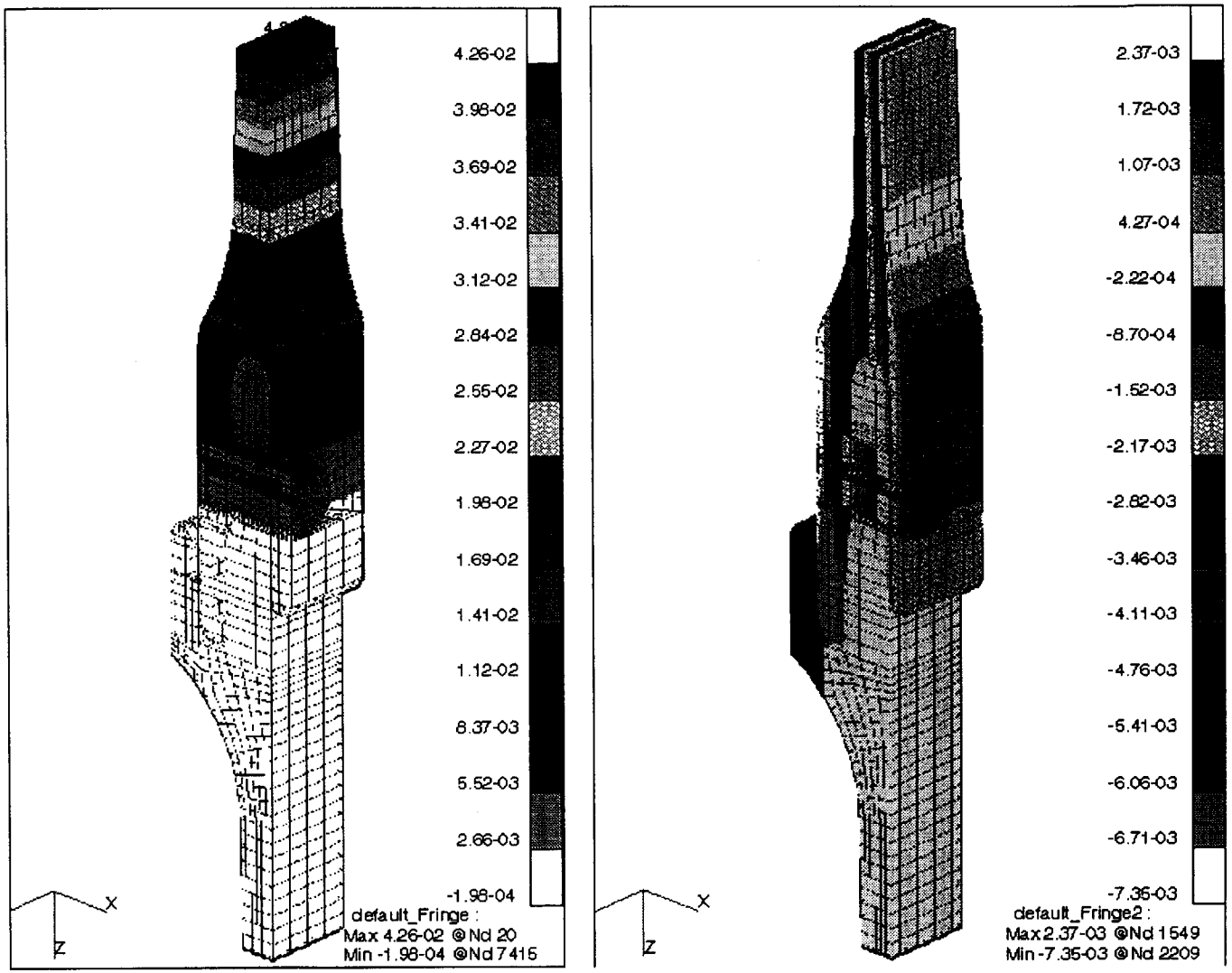

Figure A-1. a) Radial Deflection. (in.) b) Axial Deflection. (in.)

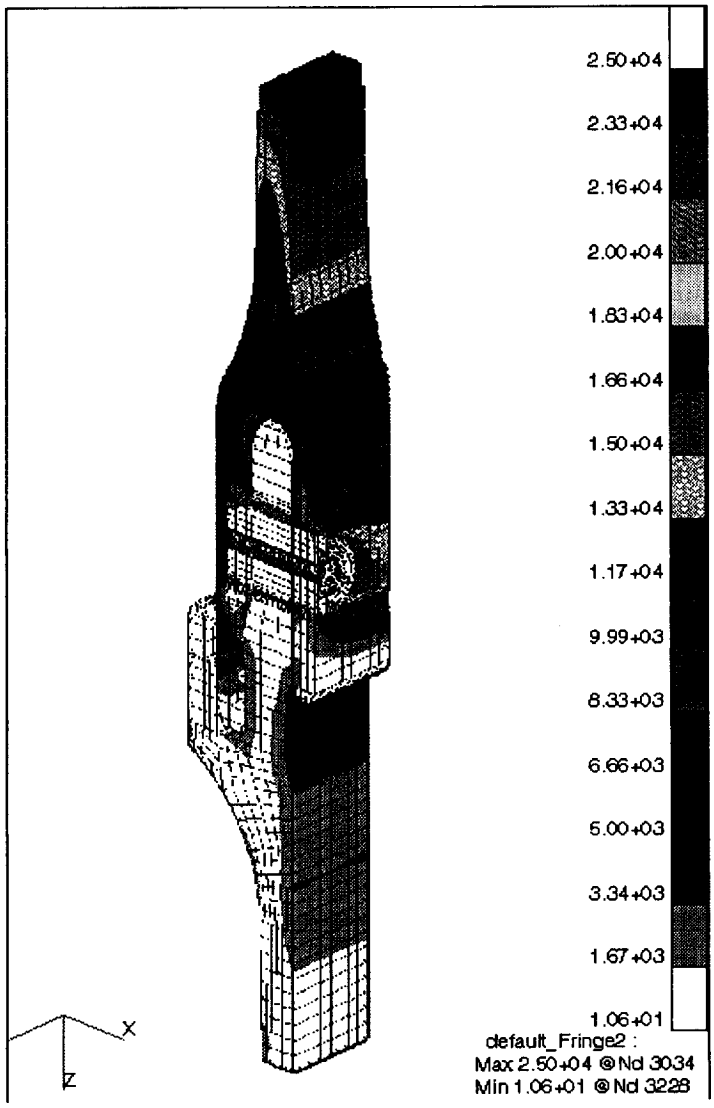

Figure A-2. Von Mises Stress Contours for Joint. (psi)

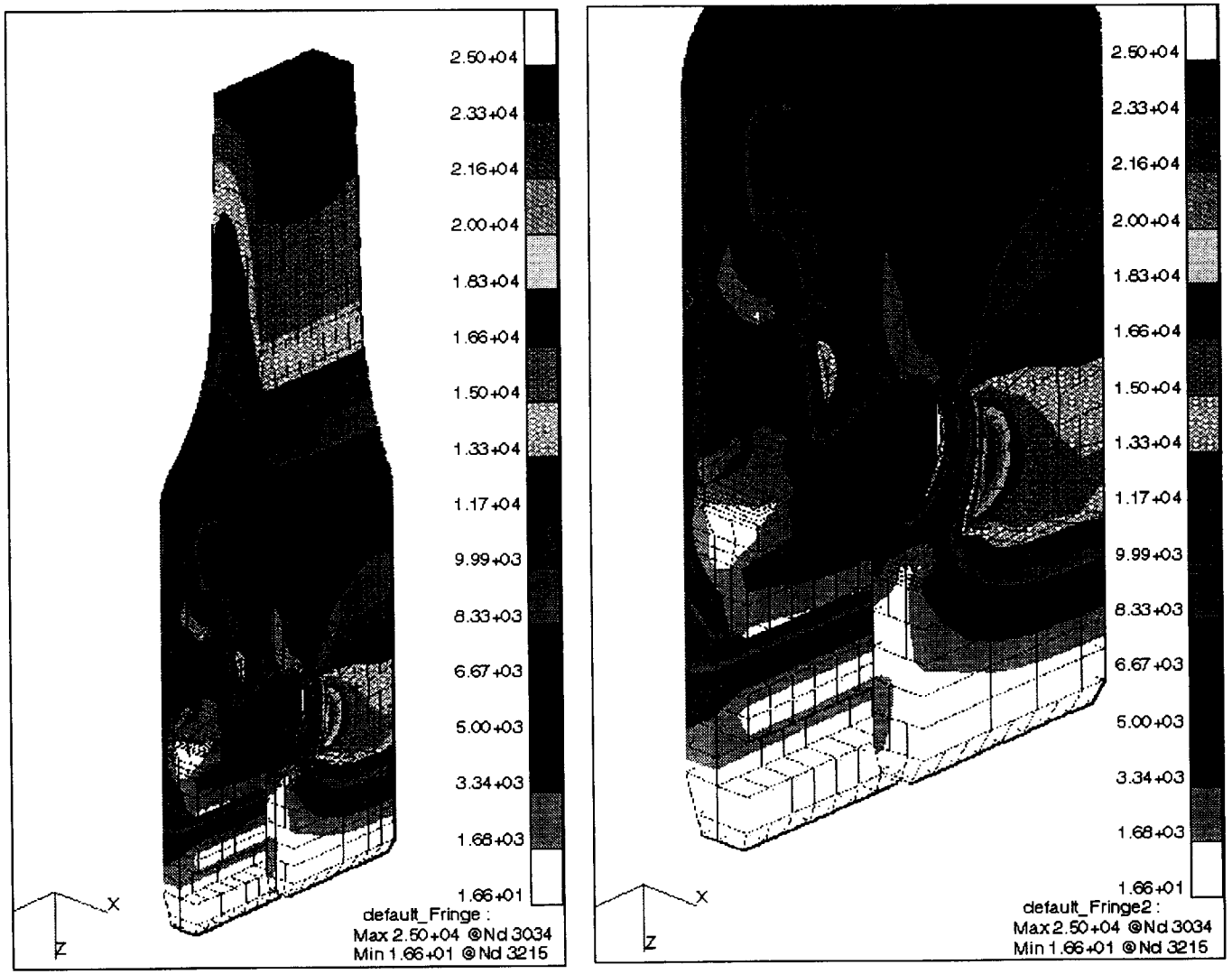

Figure A-3. Von Mises Stress Contours for Clevis. (psi)

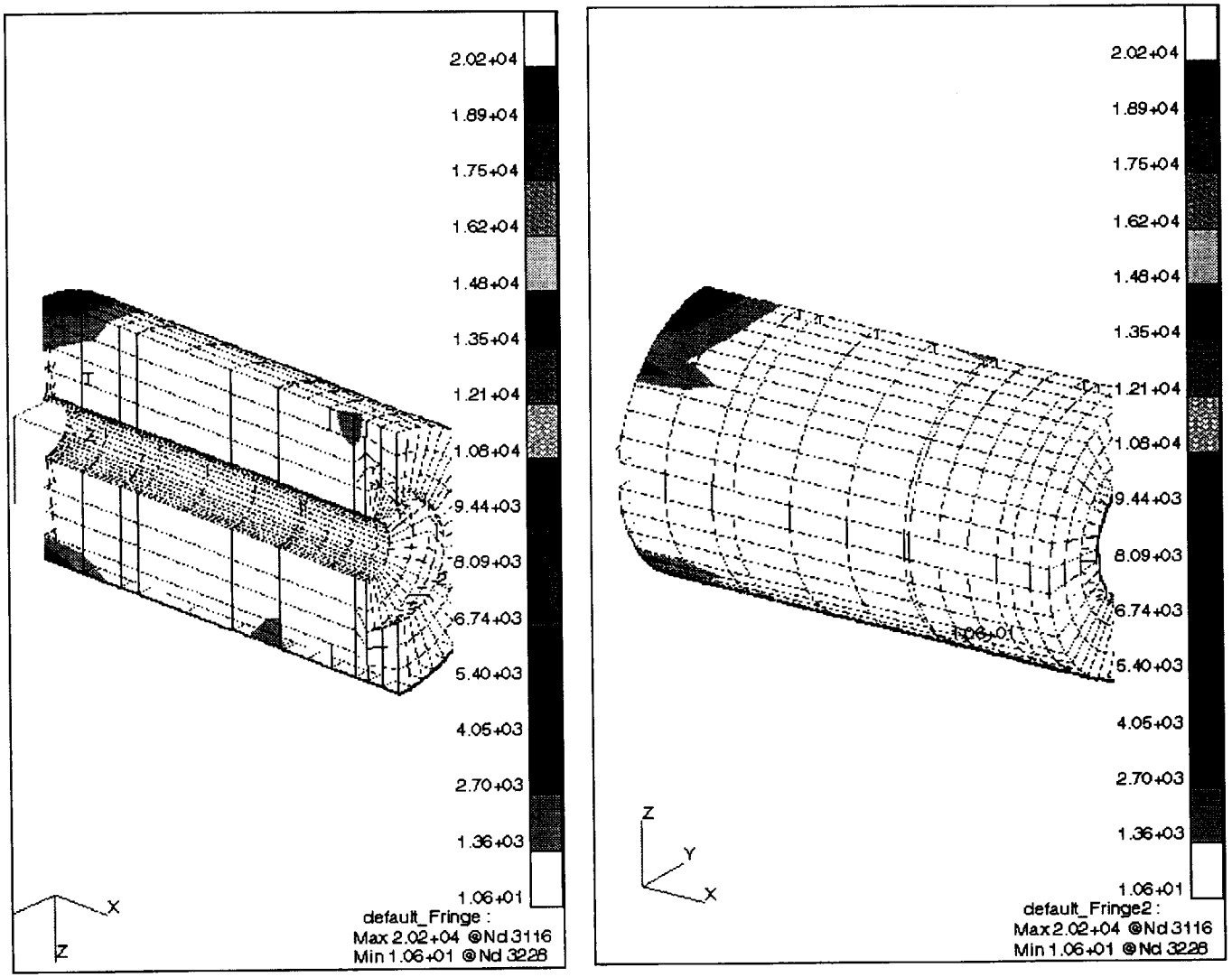

Figure A-4. Von Mises Stress Contours for Pin. (psi)

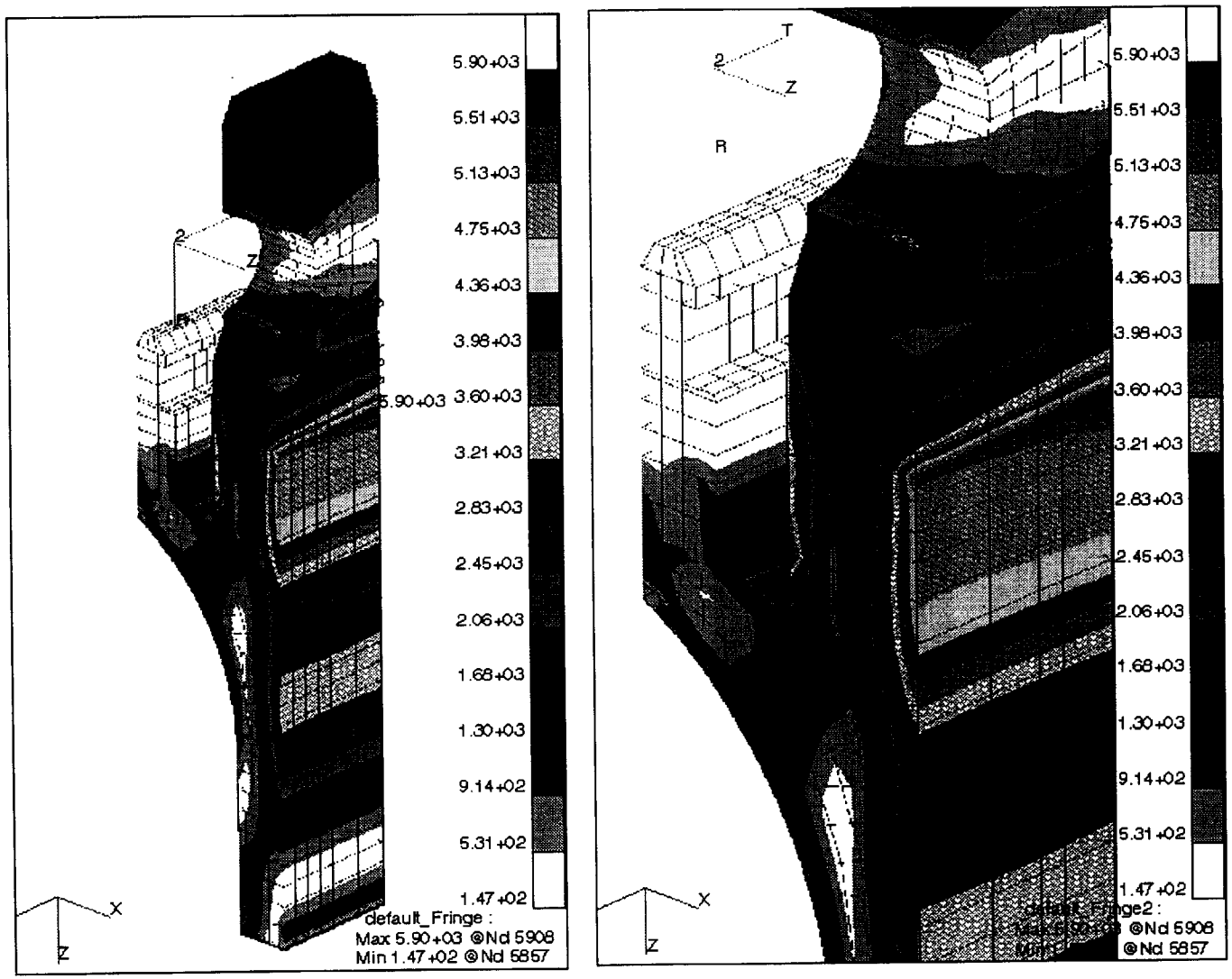

Figure A-5. Von Mises Stress Contours for Tang. (psi)

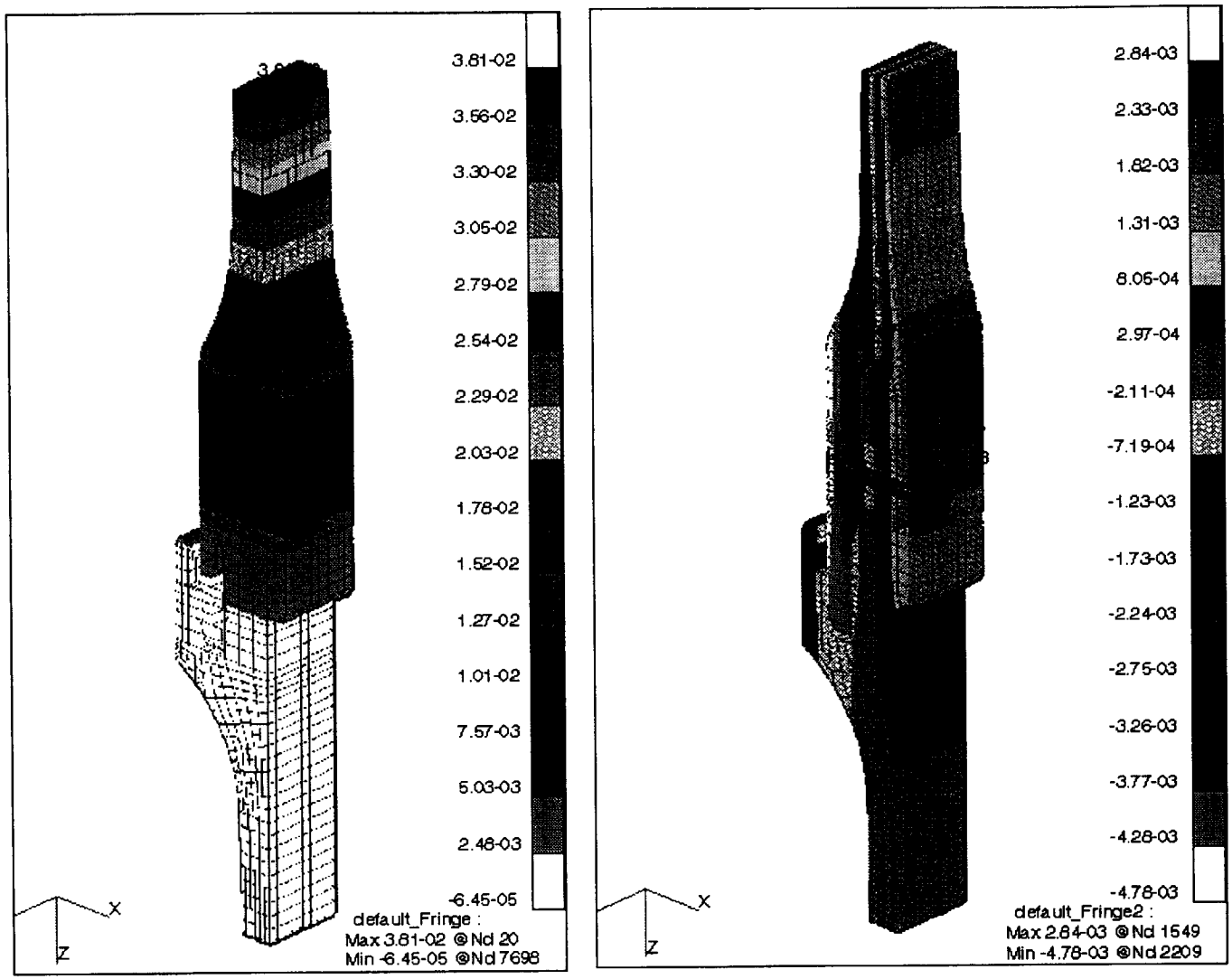

Figure A-6. a) Radial Deflection. (in.) b) Axial Deflection. (in.)

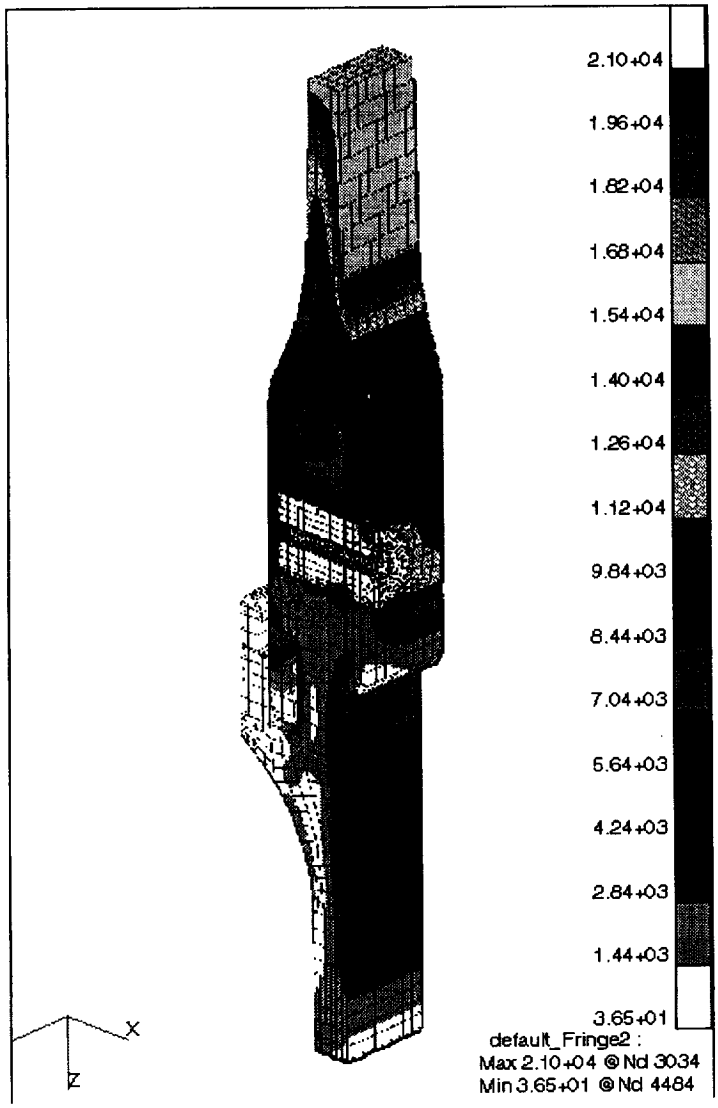

Figure A-7. Von Mises Stress Contours for Joint. (psi)

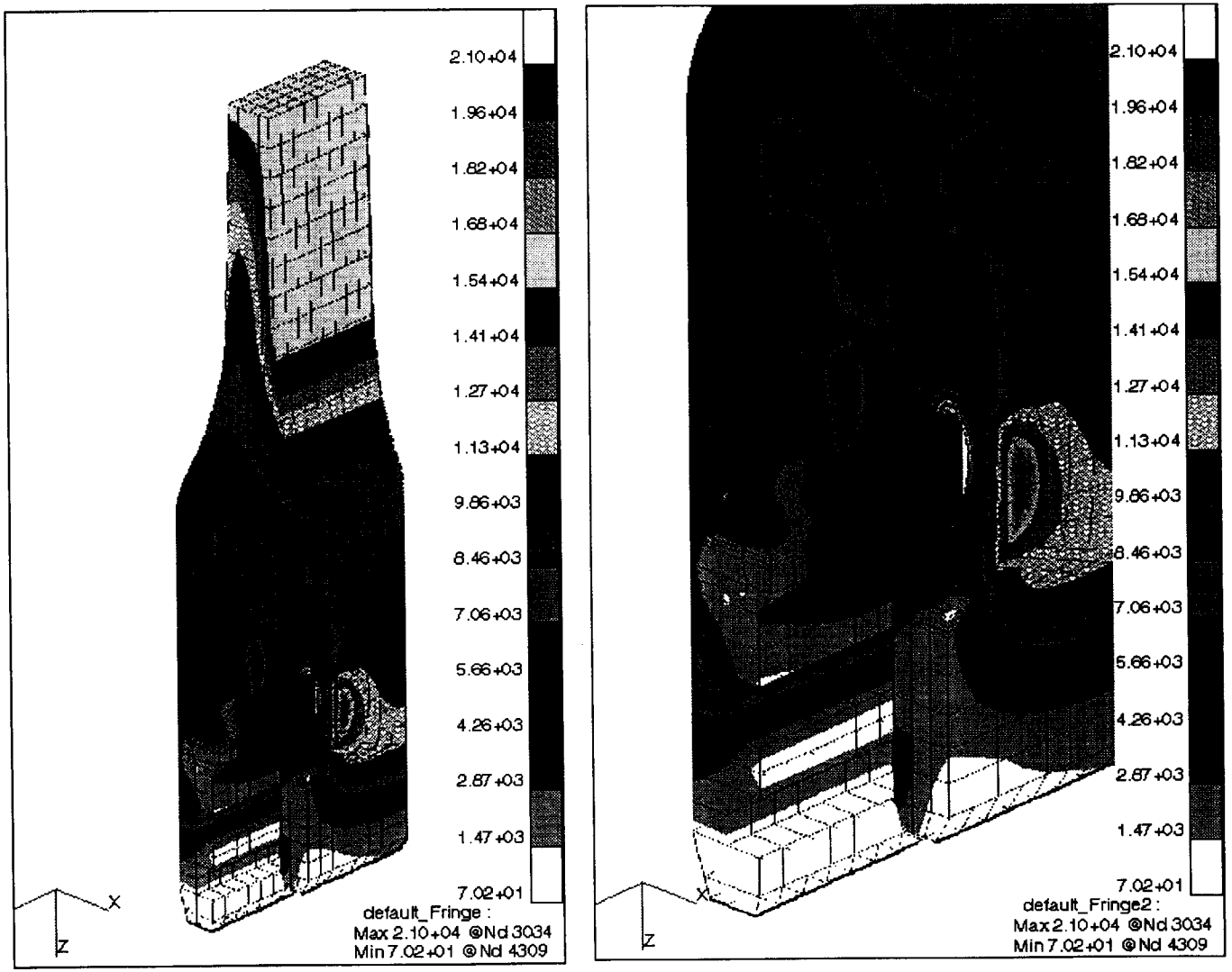

Figure A-8. Von Mises Stress Contours for Clevis. (psi)

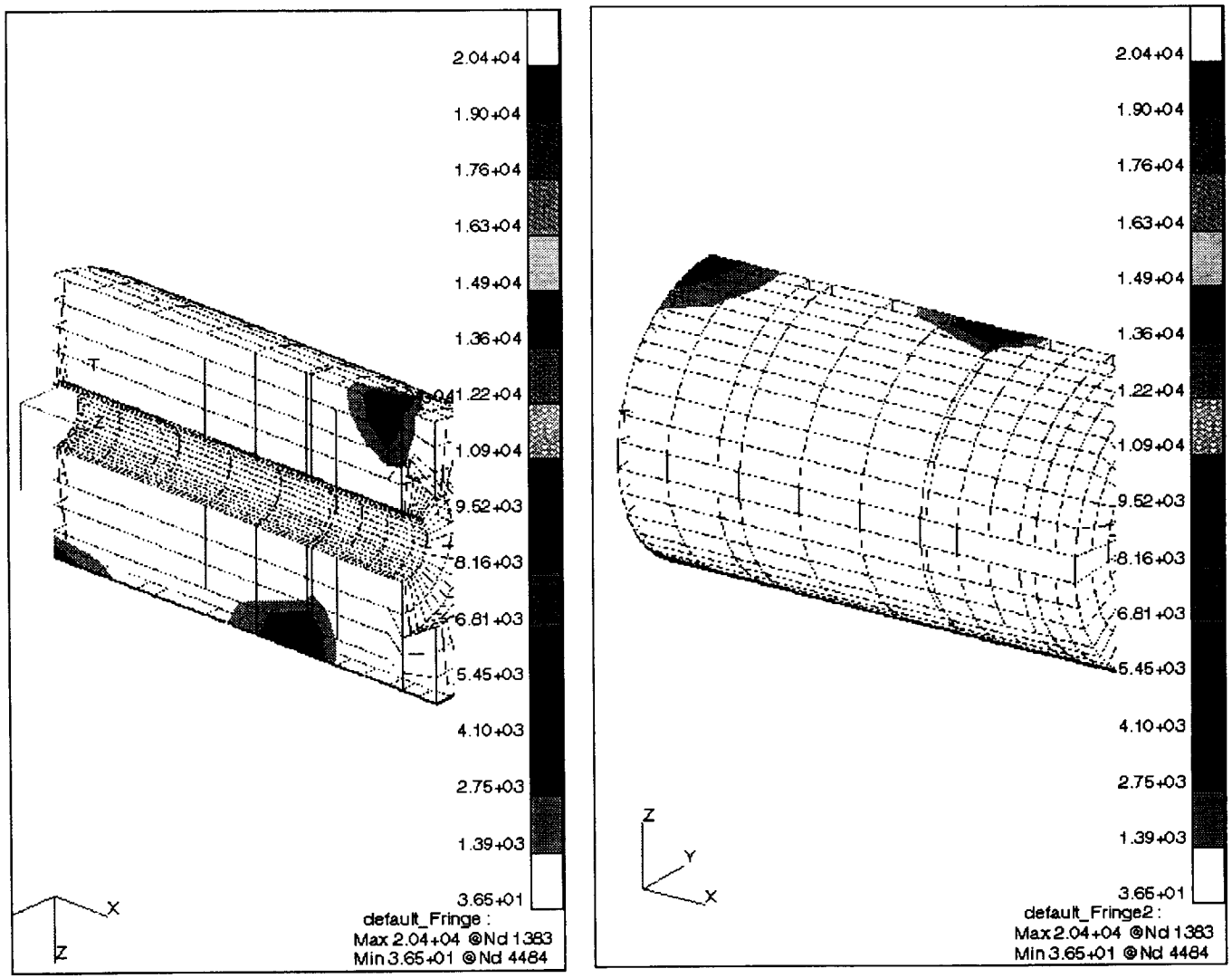

Figure A-9. Von Mises Stress Contours for Pin. (psi)

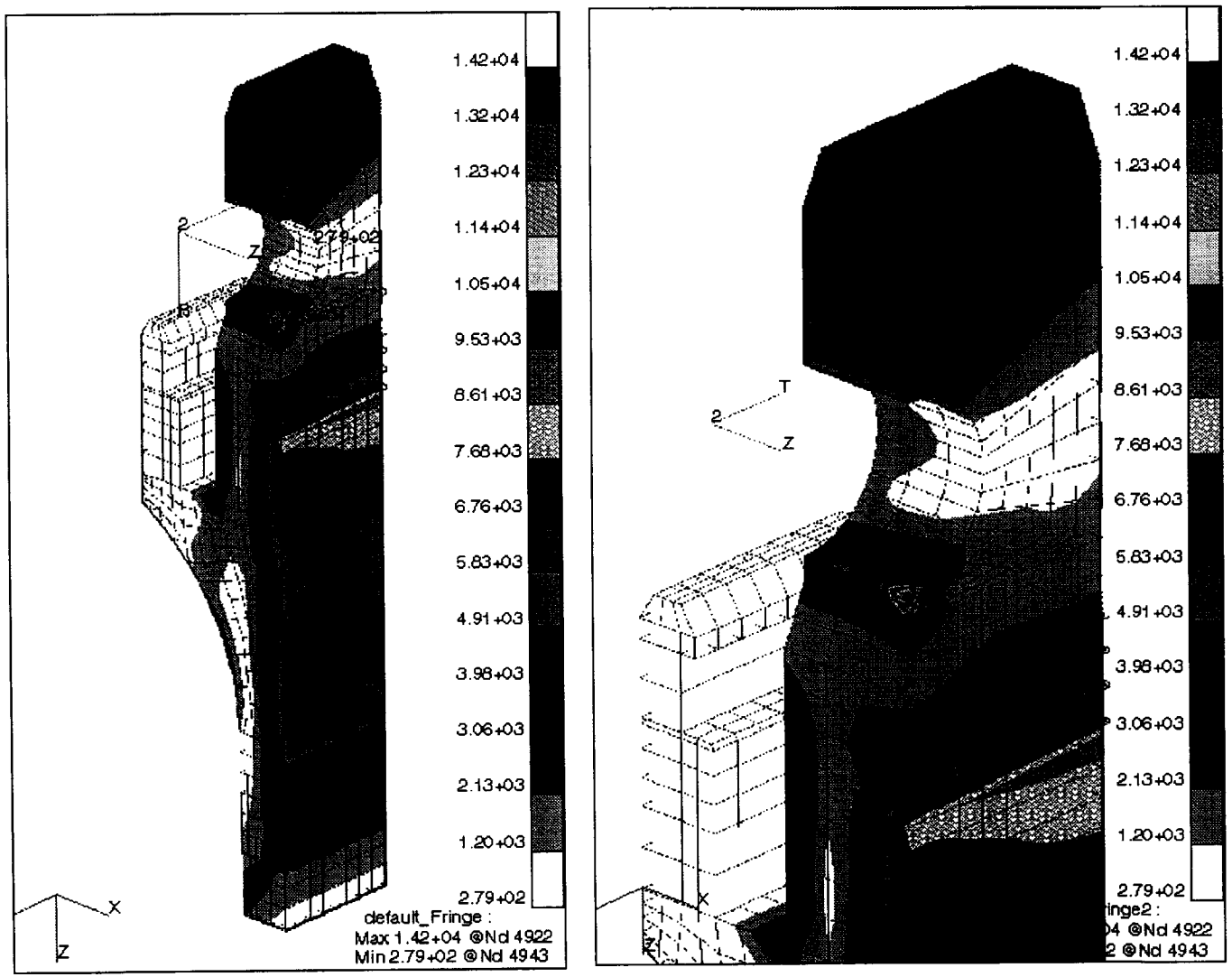

Figure A-10. Von Mises Stress Contours for Tang. (psi)

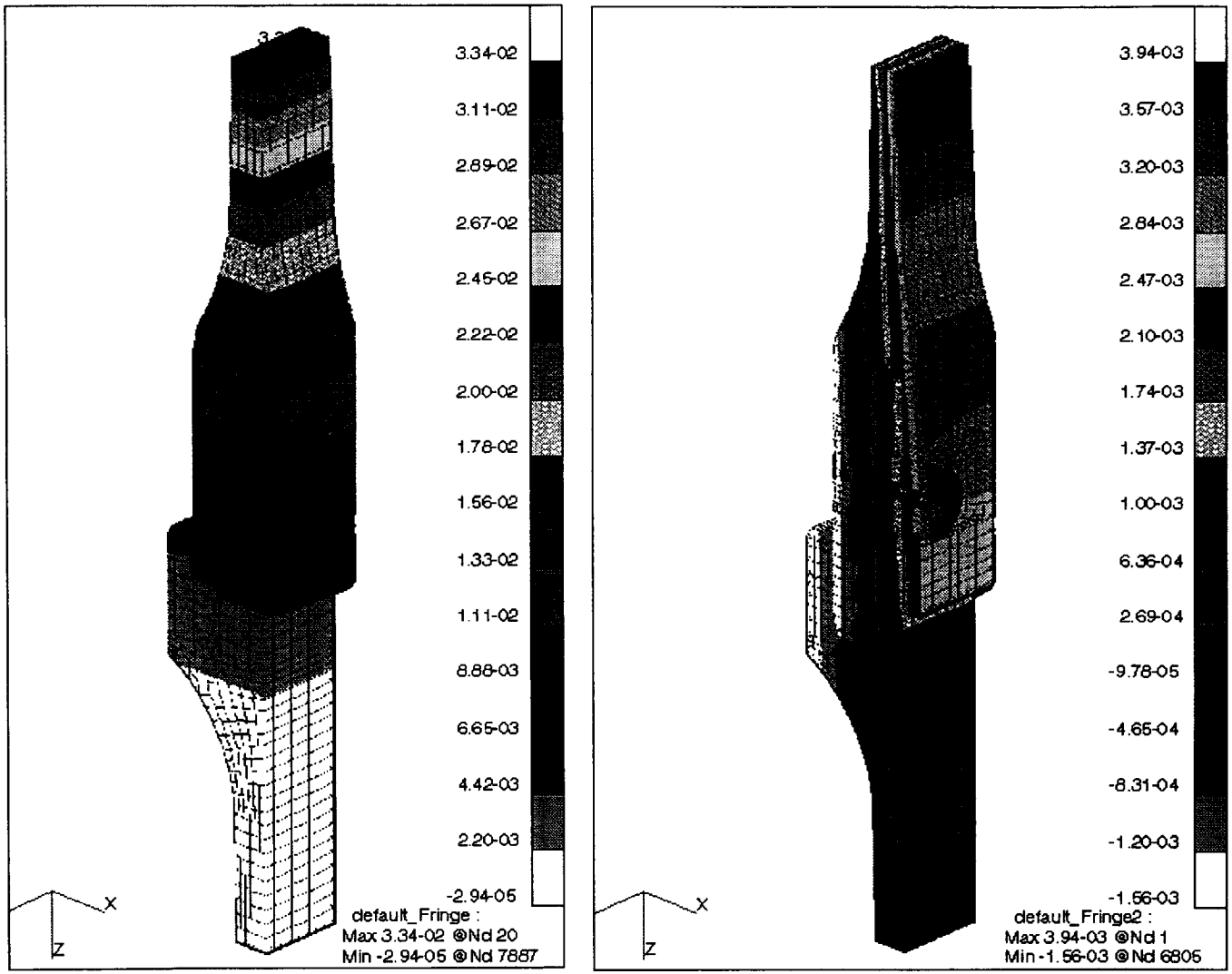

Figure A-11. a) Radial Deflection. (in.) b) Axial Deflection. (in.)

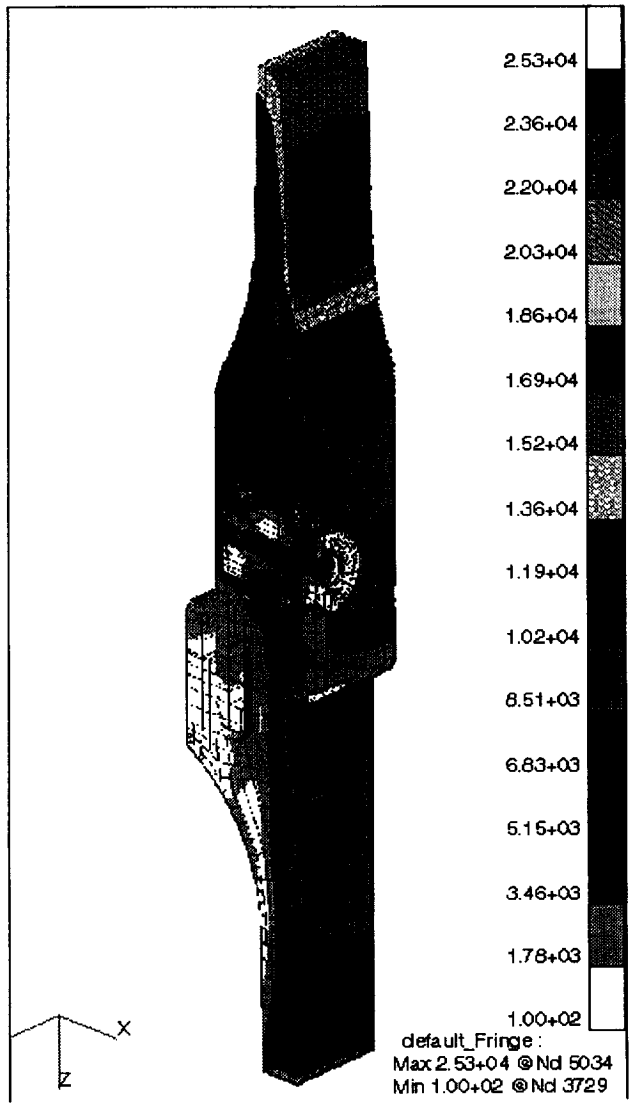

Figure A-12. Von Mises Stress Contours for Joint. (psi)

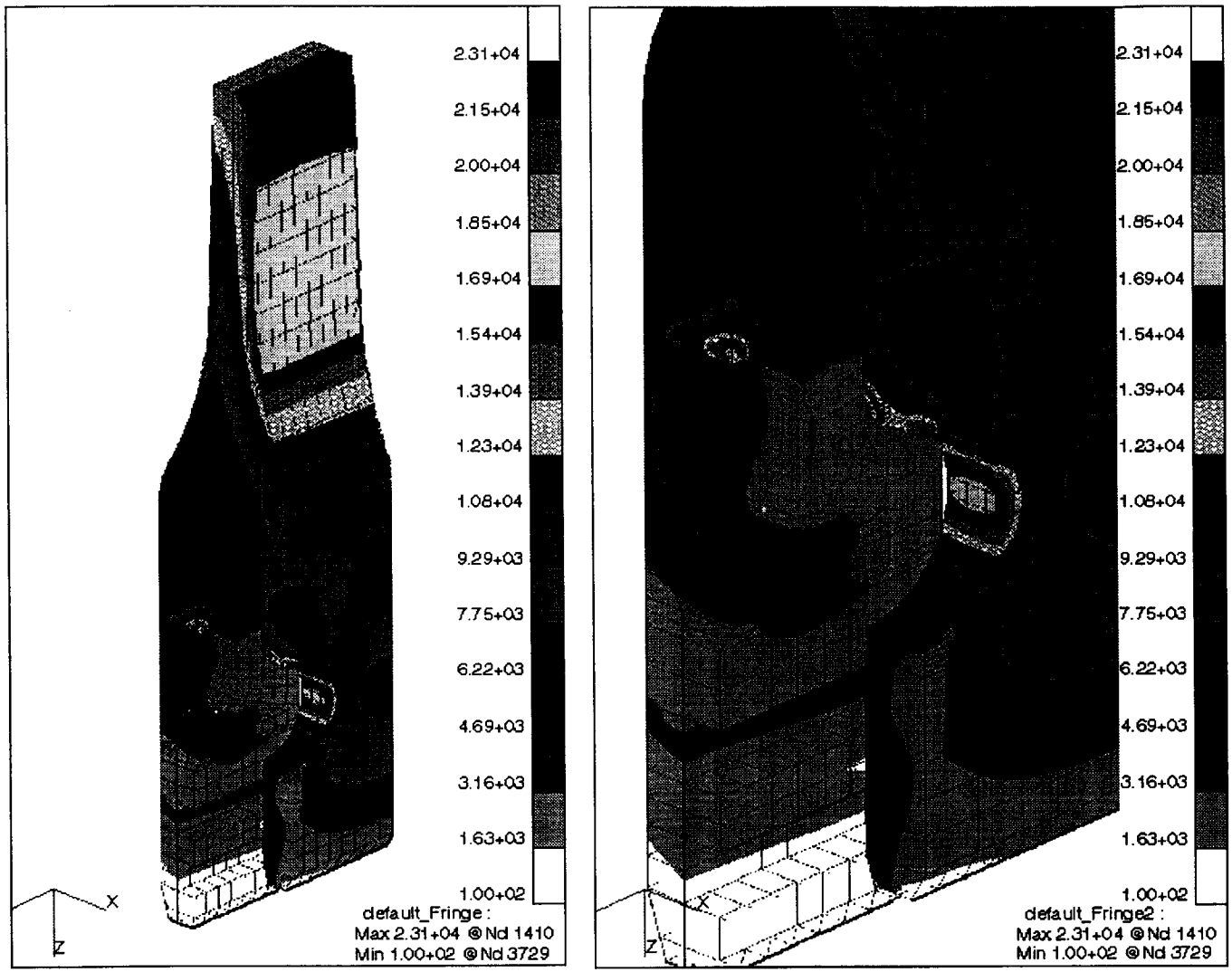

Figure A-13. Von Mises Stress Contours for Clevis. (psi)

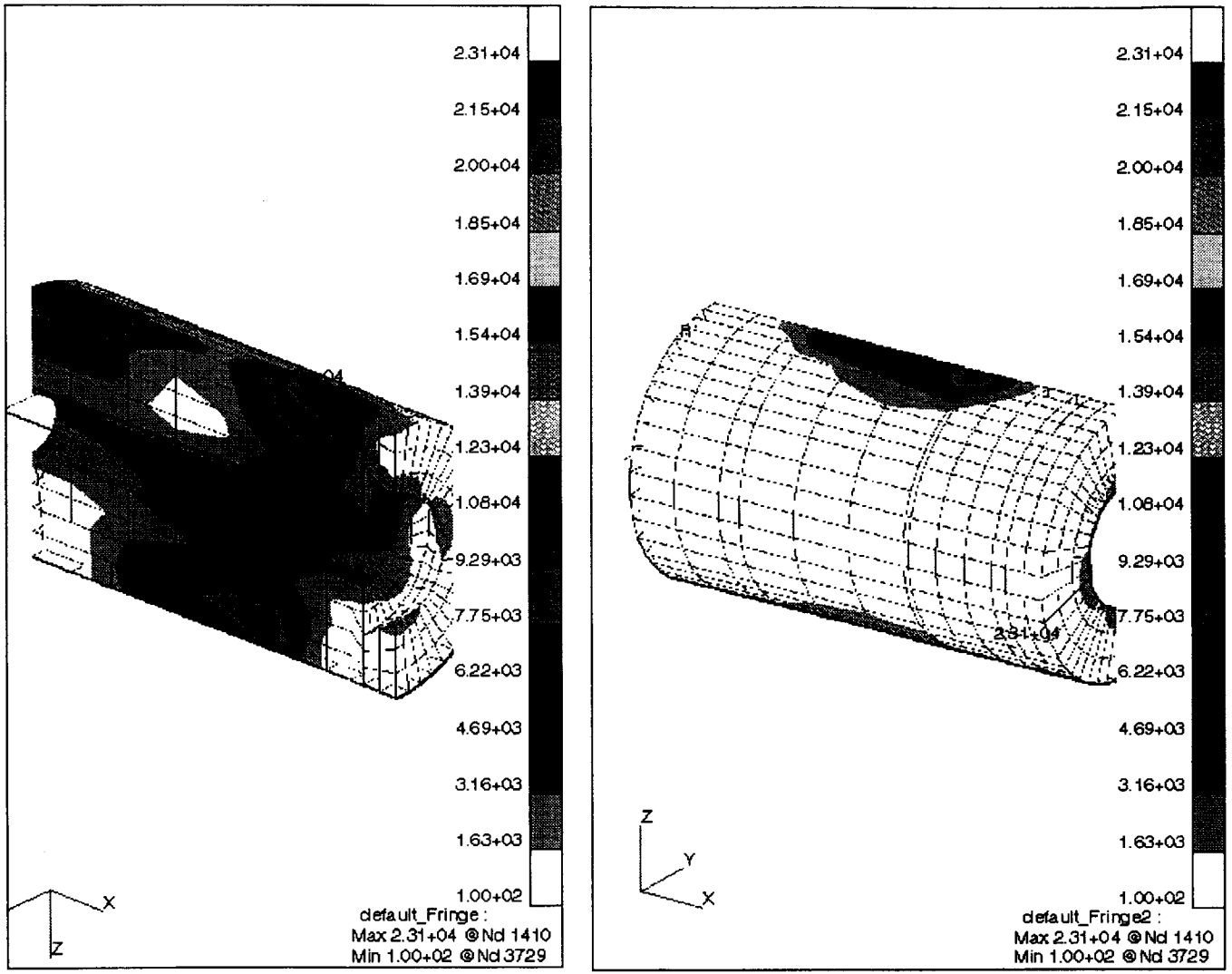

Figure A-14. Von Mises Stress Contours for Pin. (psi)

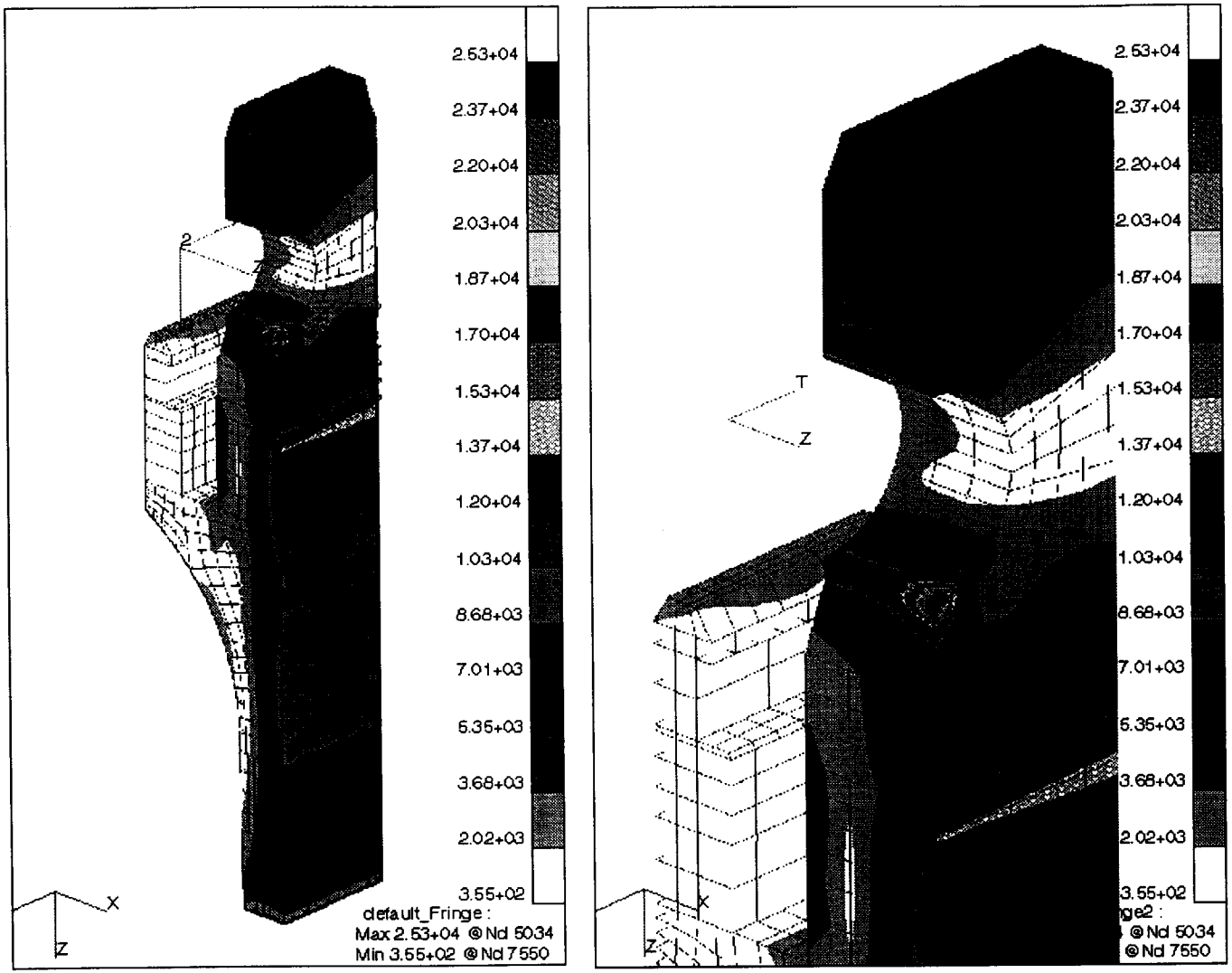

Figure A-15. Von Mises Stress Contours for Tang. (psi)

APPENDIX B

APPENDIX B

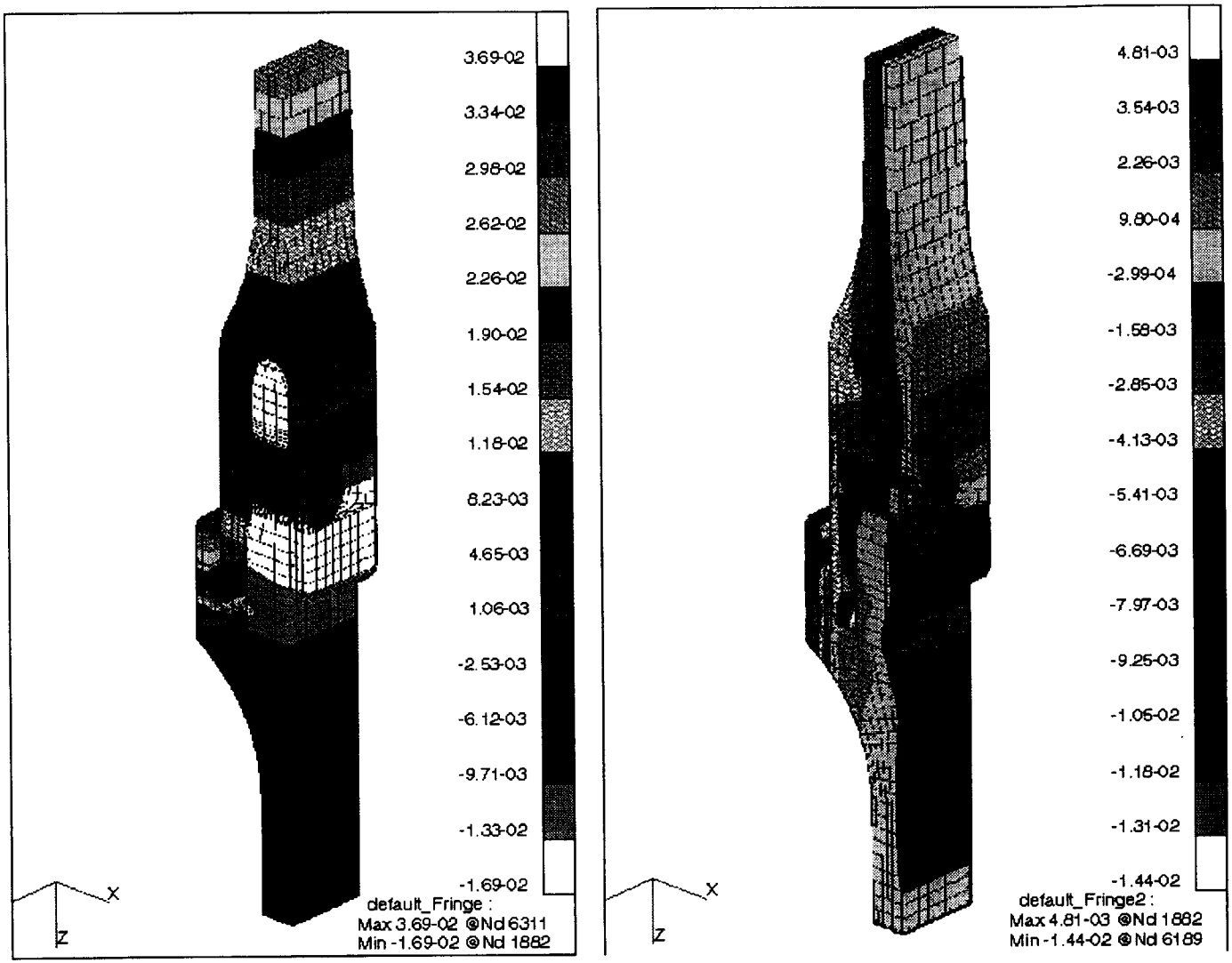

Figure B-1. a) Radial Deflection. (in.) b) Axial Deflection. (in.)

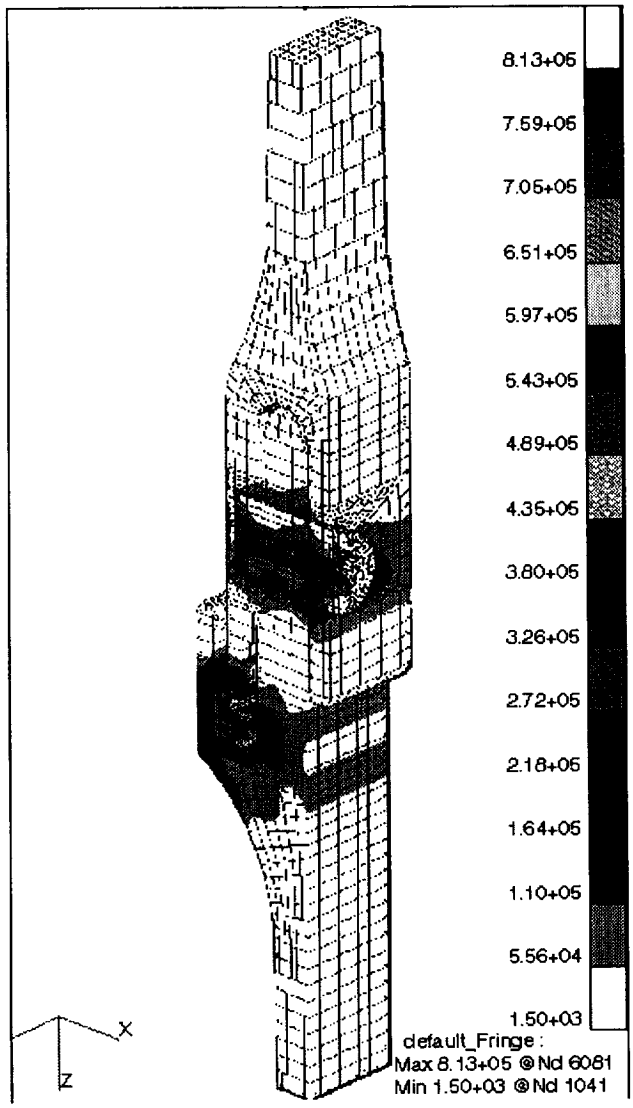

Figure B-2. Von Mises Stress Contours for Joint. (psi)

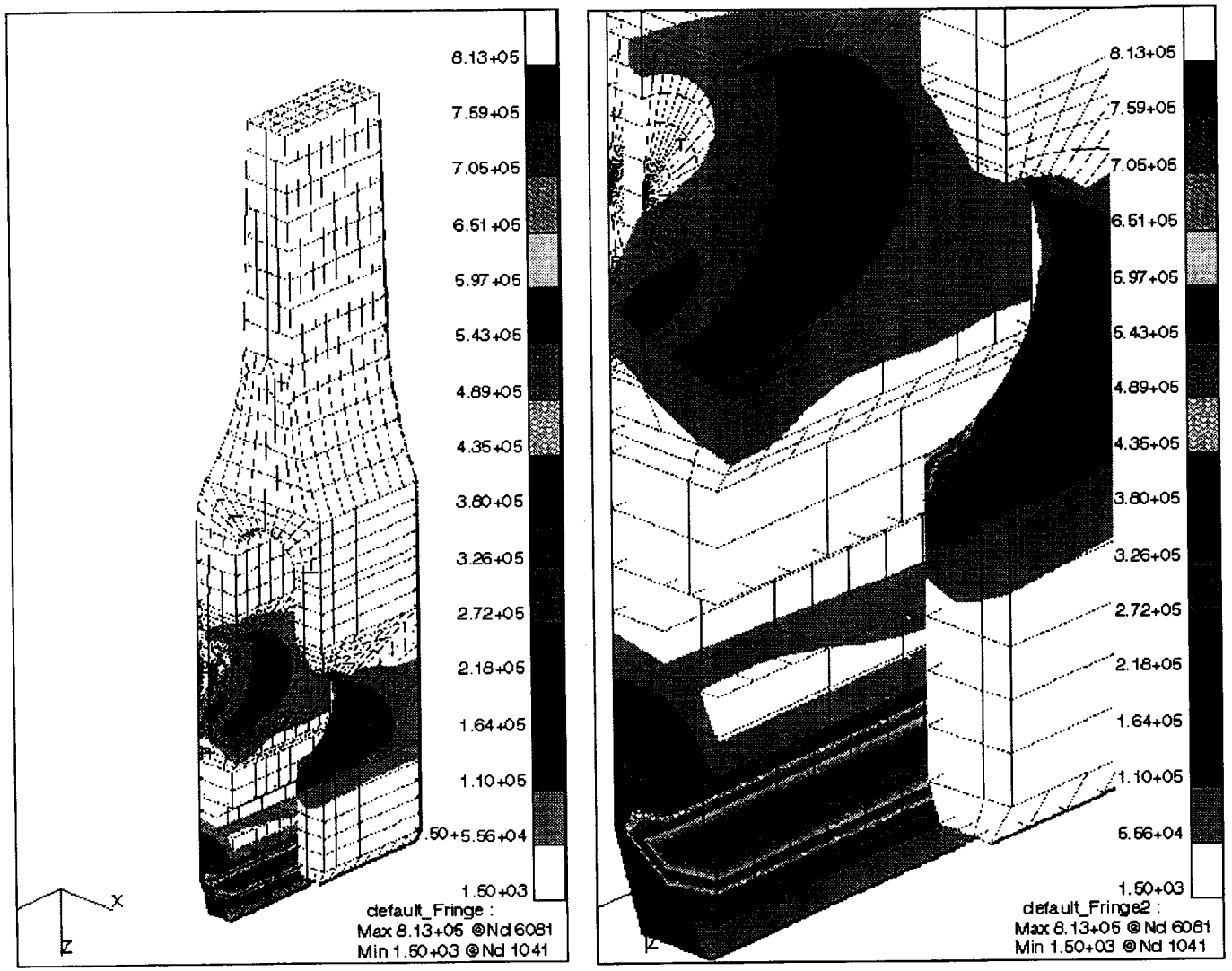

Figure B-3. Von Mises Stress Contours for Clevis. (psi)

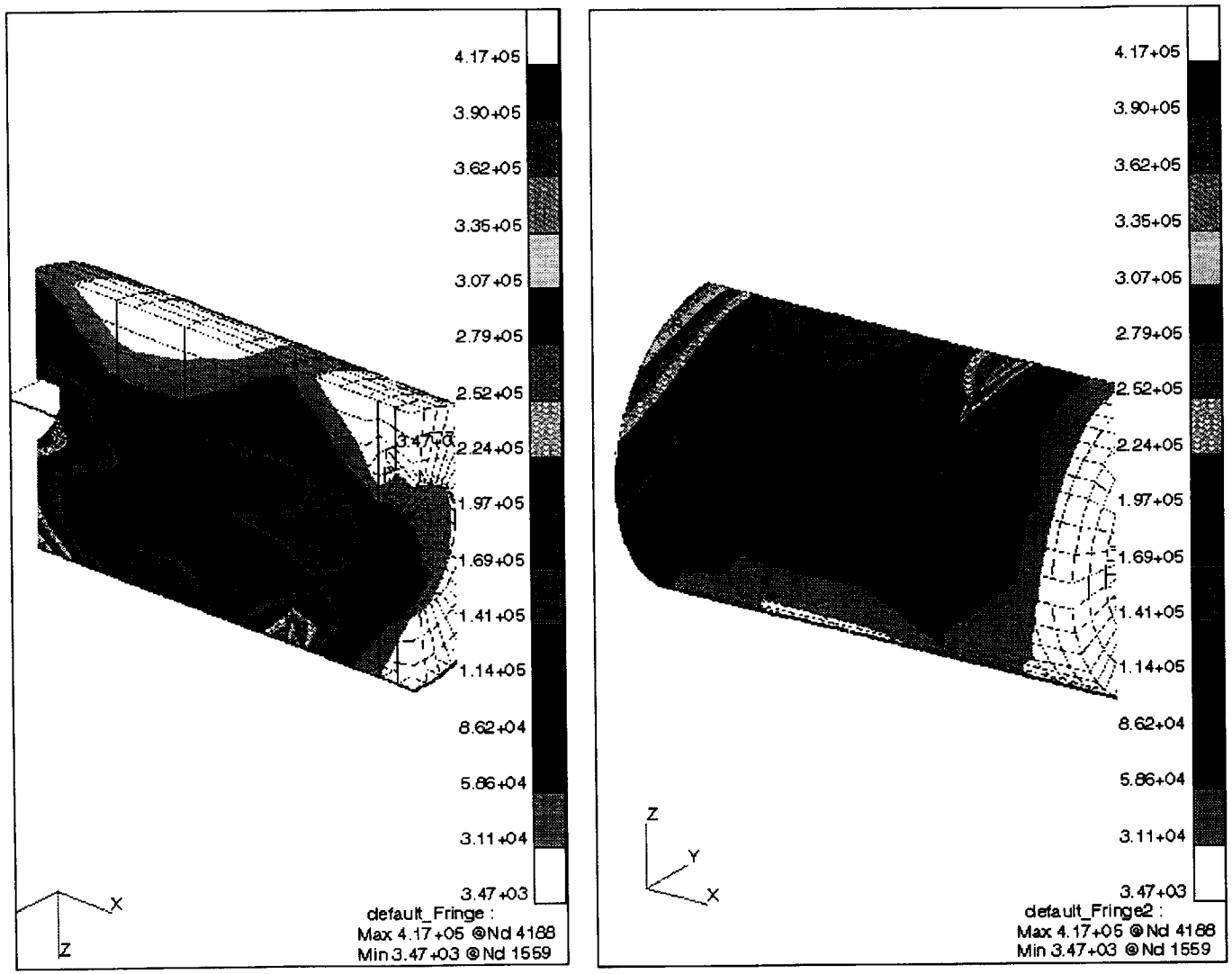

Figure B-4. Von Mises Stress Contours for Pin. (psi)

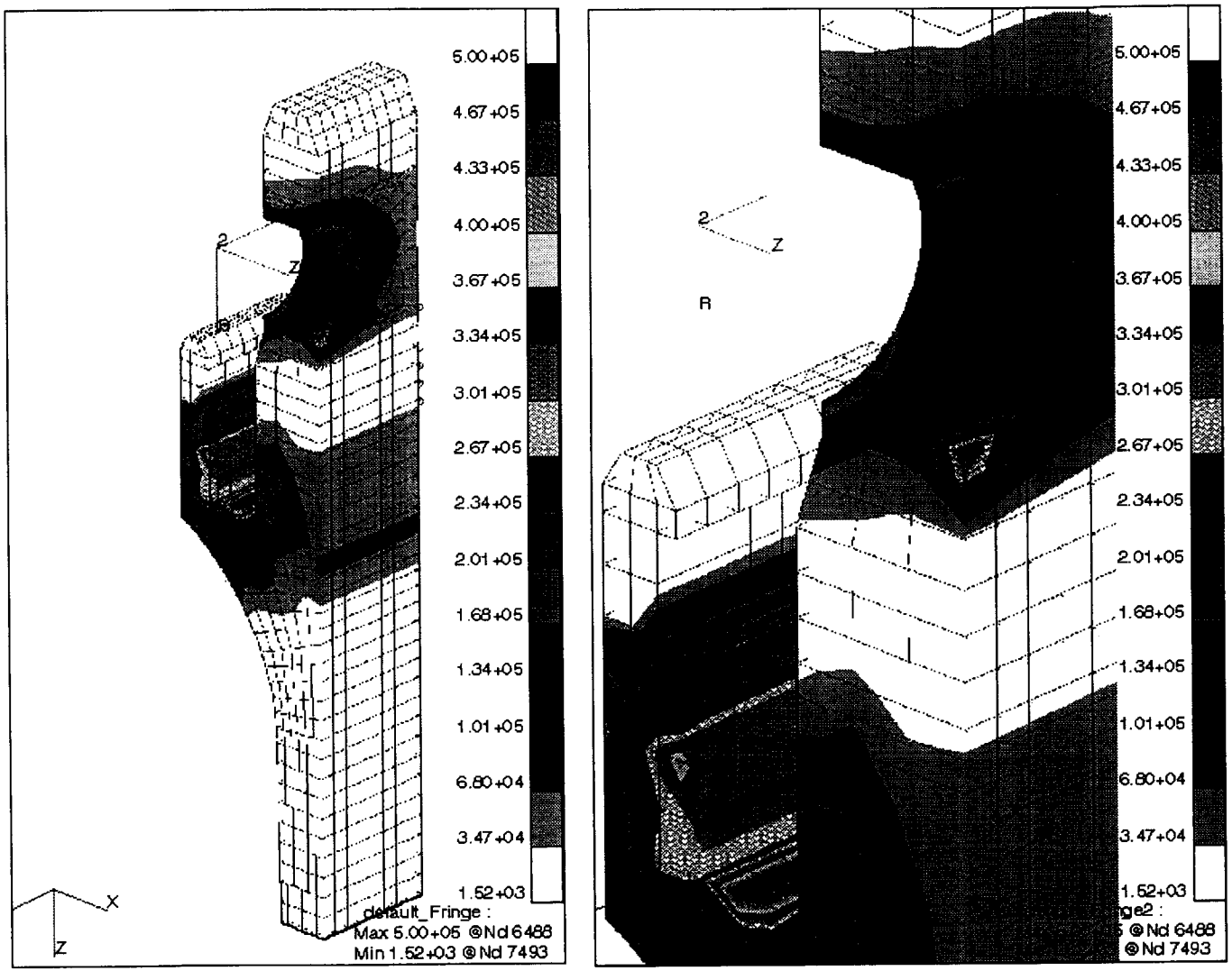

Figure B-5. Von Mises Stress Contours for Tang. (psi)

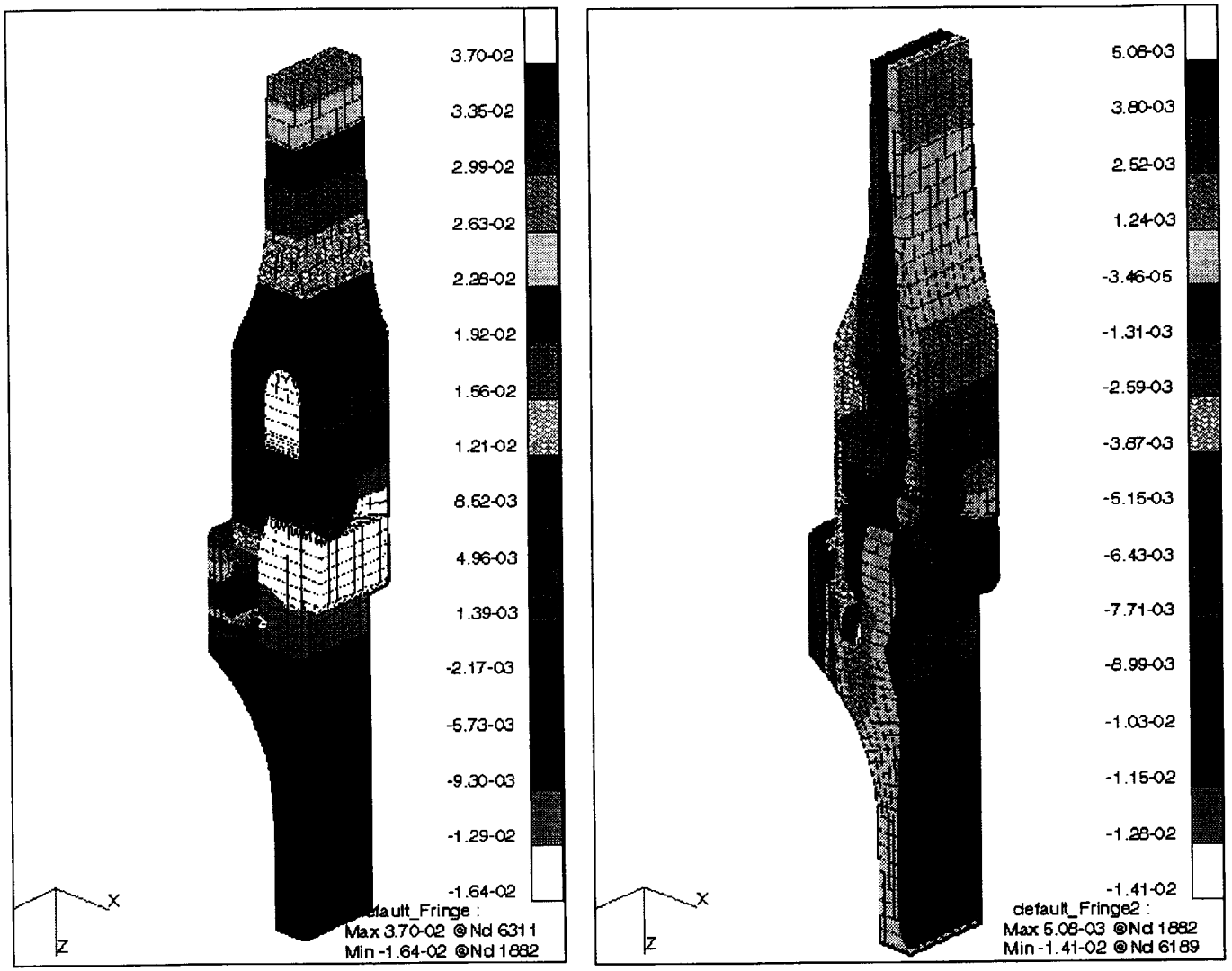

Figure B-6. a) Radial Deflection (in.) b) Axial Deflection (in.)

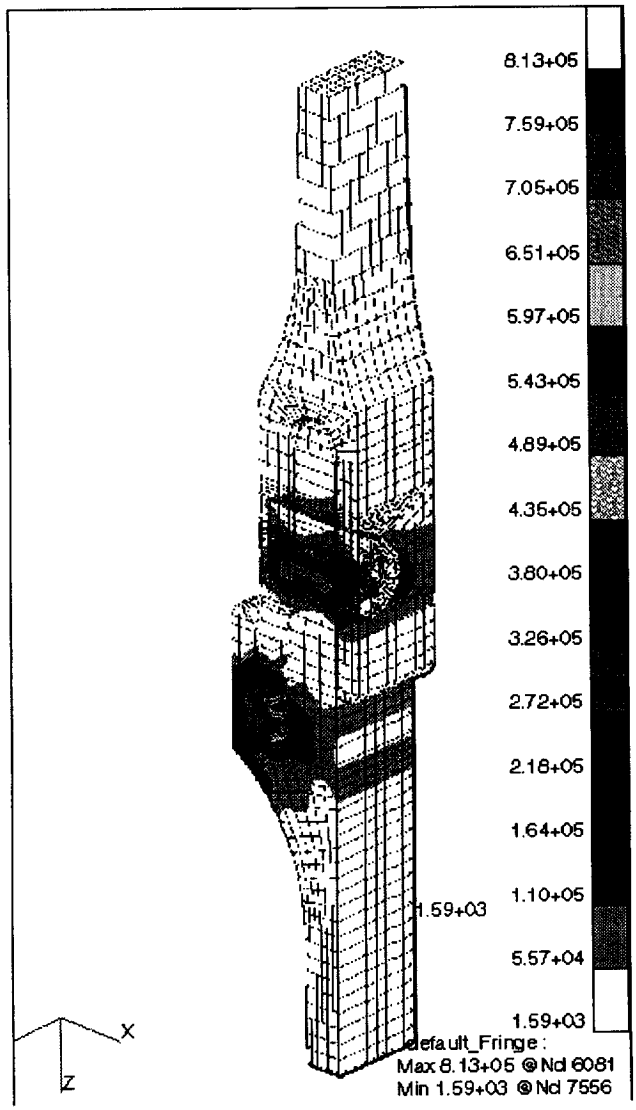

Figure B-7. Von Mises Stress Contours for Joint. (psi)

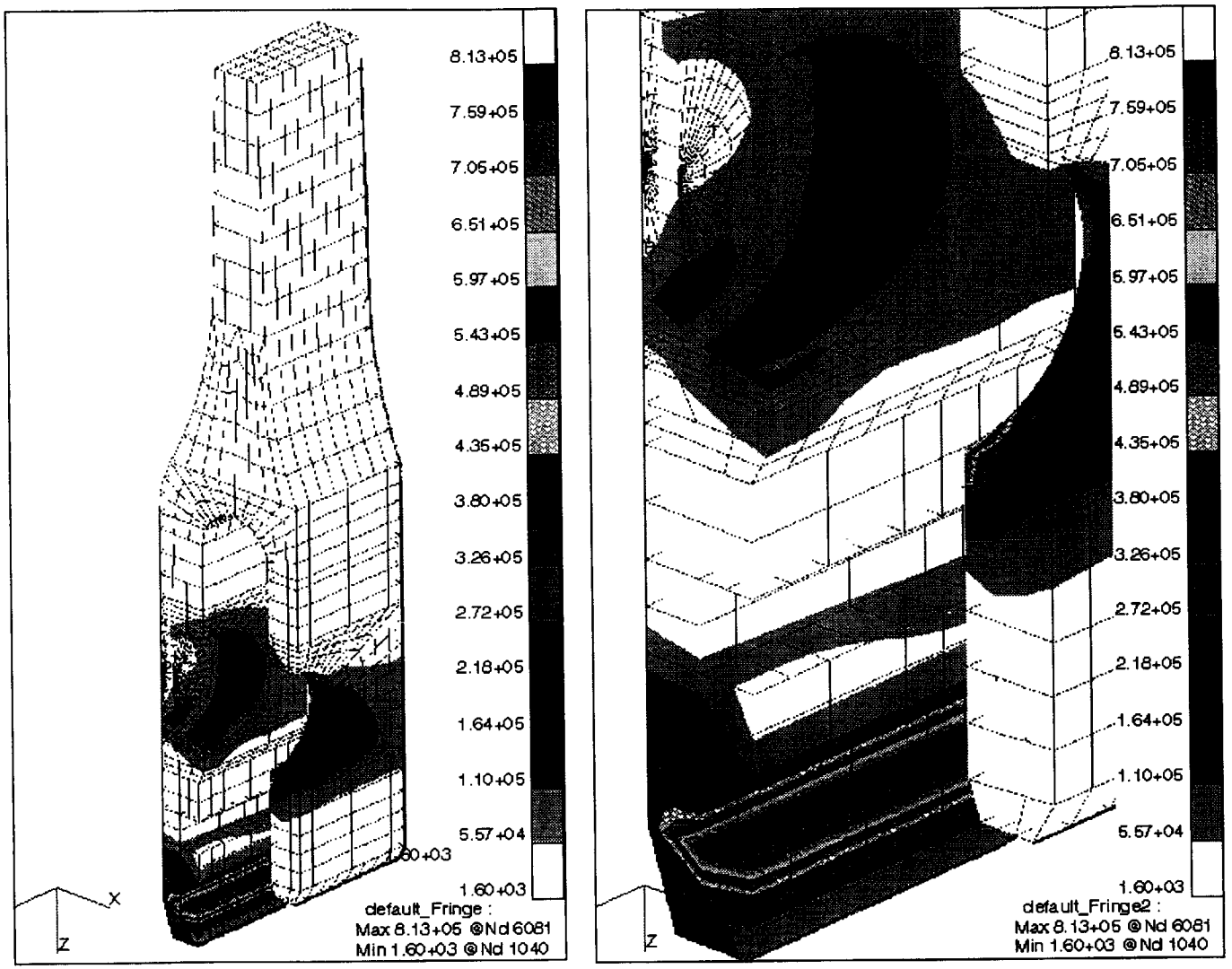

Figure B-8. Von Mises Stress Contours for Clevis. (psi)

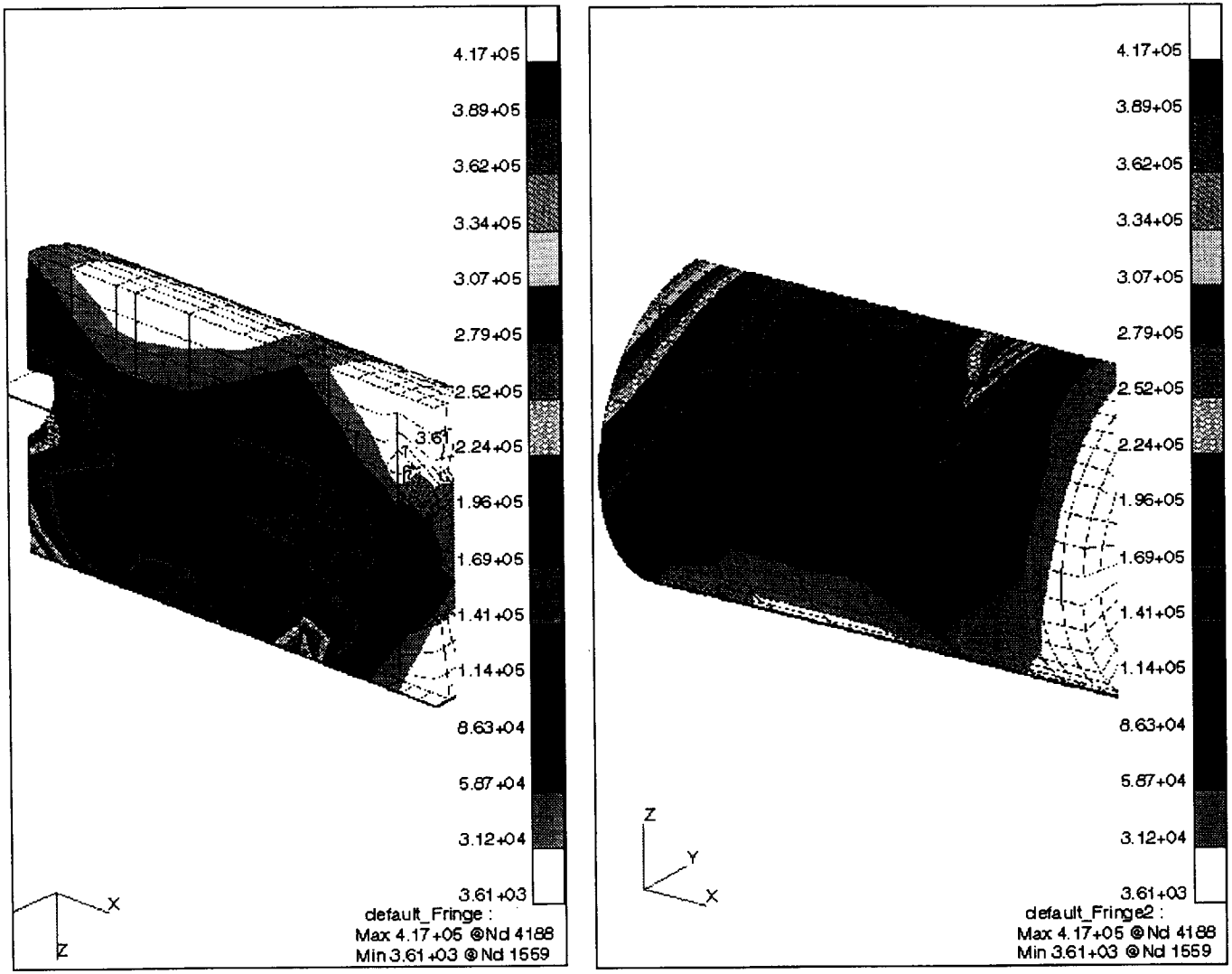

Figure B-9. Von Mises Stress Contours for Pin. (psi)

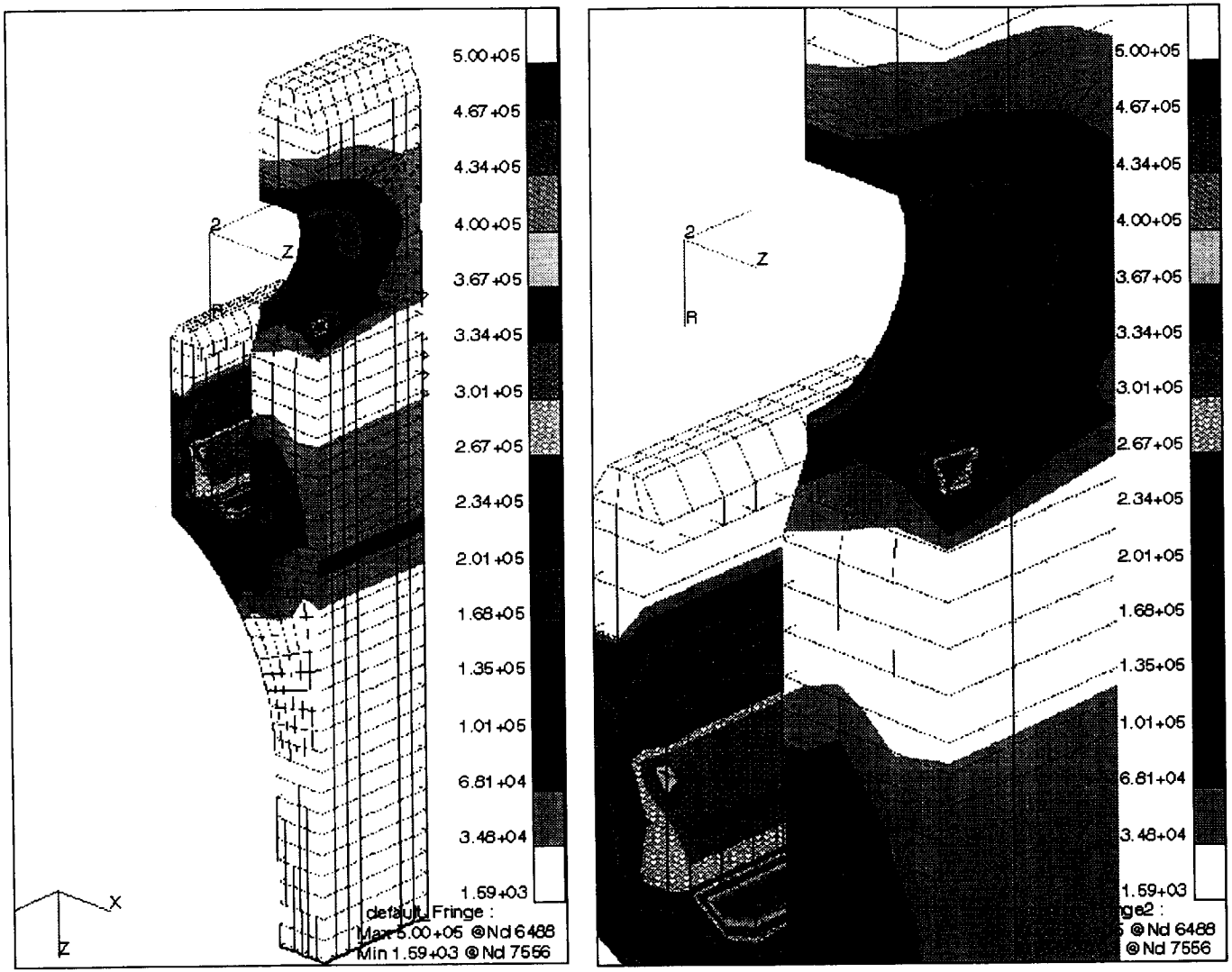

Figure B-10. Von Mises Stress Contours for Tang. (psi)

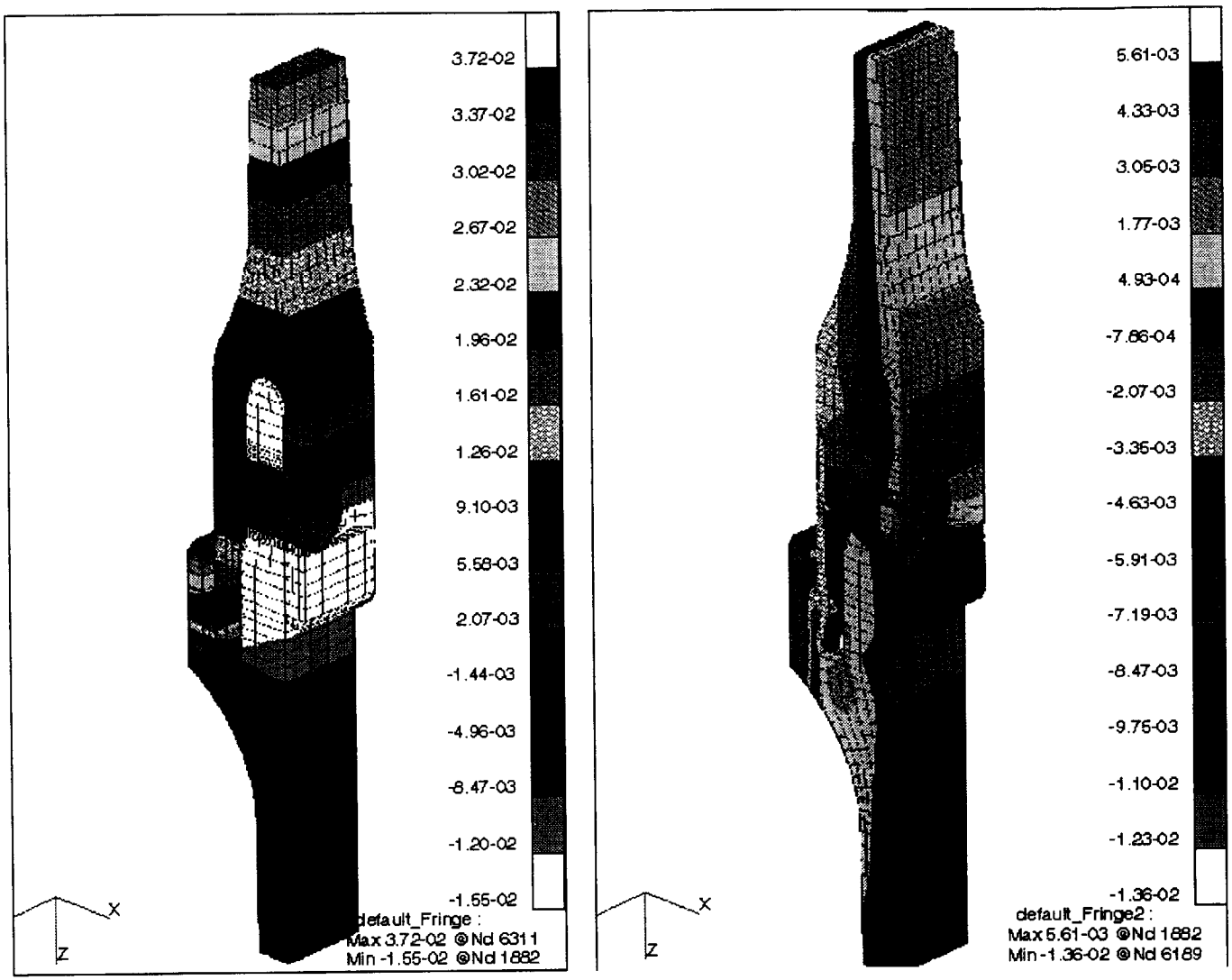

Figure B-11. a) Radial Deflection (in.) b) Axial Deflection (in.)

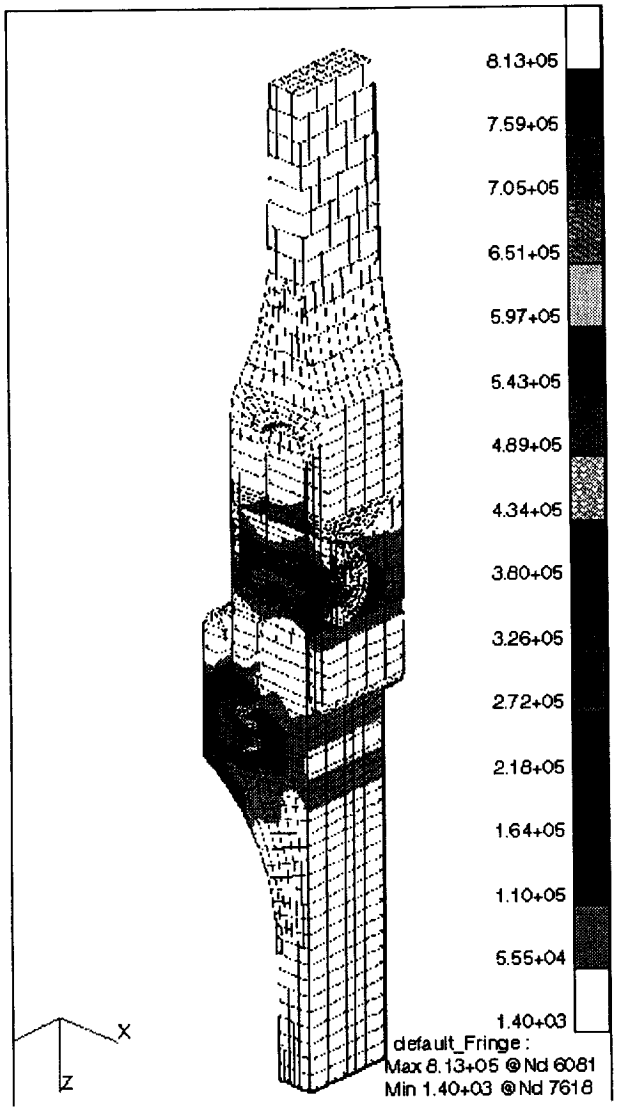

Figure B-12. Von Mises Stress Contours for Joint. (psi)

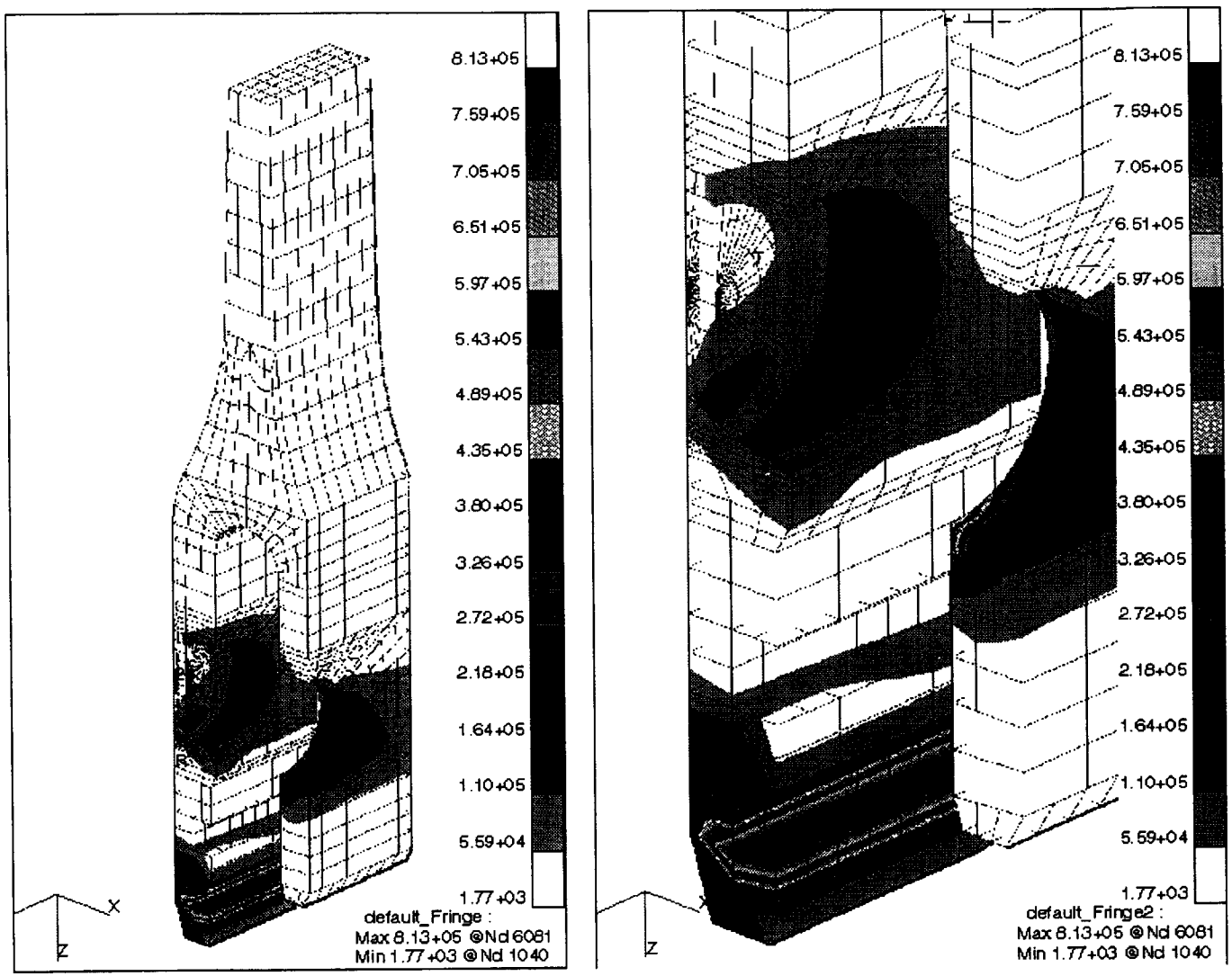

Figure B-13. Von Mises Stress Contours for Clevis. (psi)

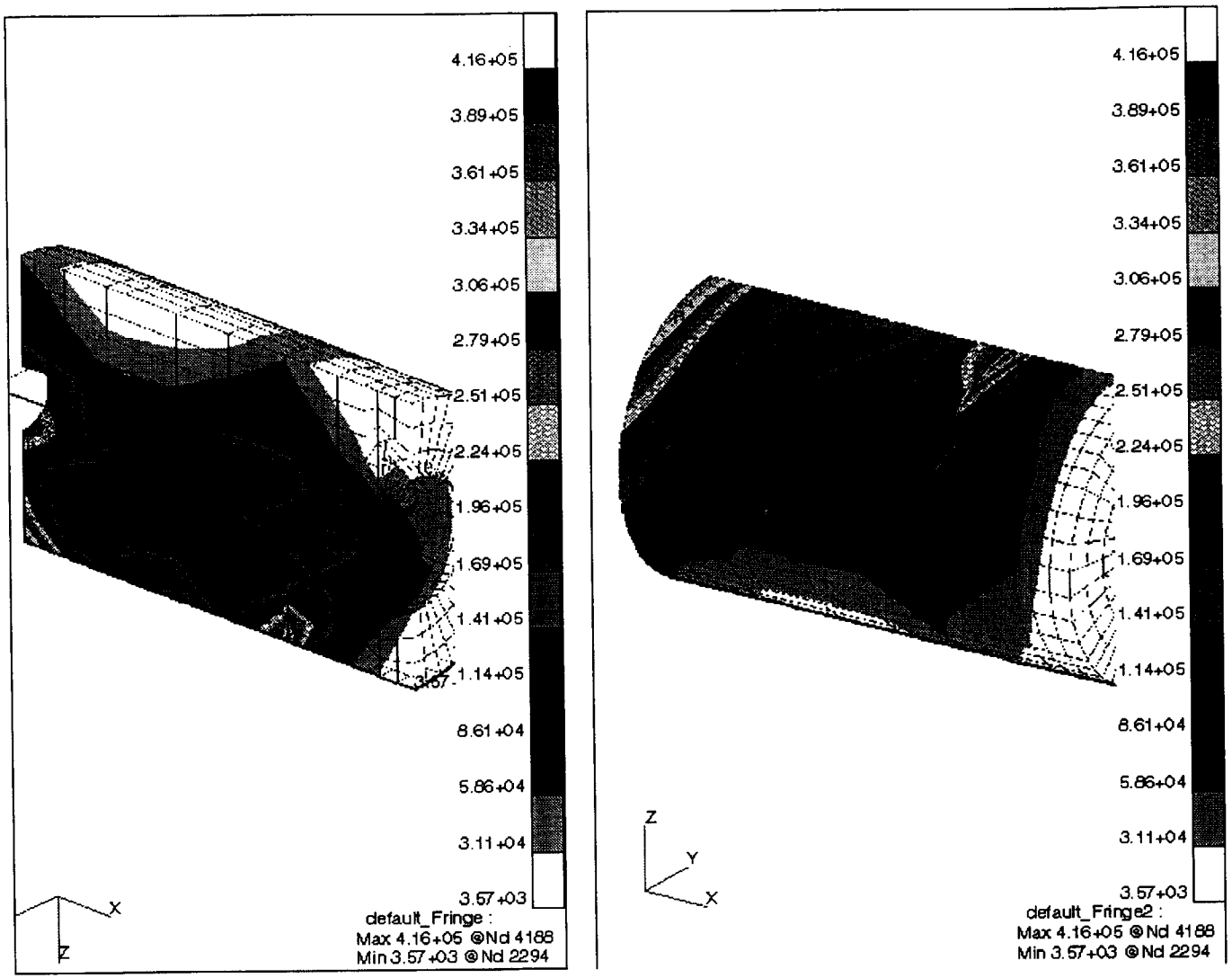

Figure B-14. Von Mises Stress Contours for Pin. (psi)

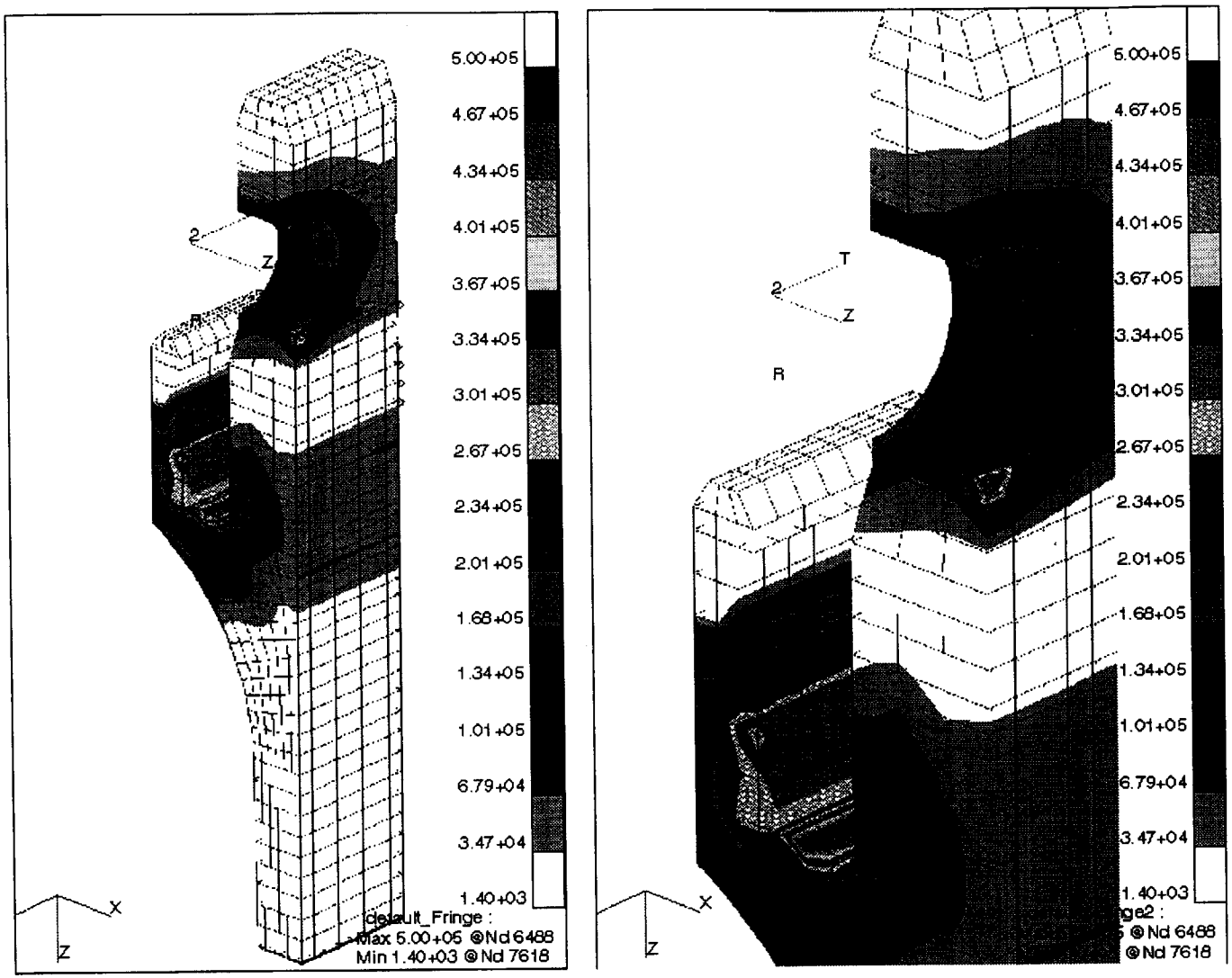

Figure B-15. Von Mises Stress Contours for Tang. (psi)